PNNL-30041 Rev. 1

Light Water Reactor Sustainability Program

Sequential Versus Simultaneous Aging of XLPE and EPDM Nuclear Cable Insulation Subjected to Elevated Temperature and Gamma Radiation (Final Results)

December 2020

U.S. Department of Energy

Office of Nuclear Energy

PNNL-30041 Rev. 1

Sequential Versus Simultaneous Aging of XLPE and EPDM Nuclear Cable Insulation Subjected to Elevated Temperature and Gamma Radiation (Final Results)

Leonard S. Fifield, Mychal P. Spencer, Yelin Ni, Donghui Li, Madhusudhan R. Pallaka, Tucker T. Bisel, Andy Zwoster, Mark K. Murphy

Milestone 21OR0404015

December 2020

Prepared for the
U.S. Department of Energy
Office of Nuclear Energy

SUMMARY

This report addresses one of the knowledge gaps identified for prediction of nuclear electrical cable aging: the conservatism of accelerated aging performed during historical cable qualification. If synergistic effects—degradation mechanisms unique to simultaneous exposure to thermal and gamma radiation stress—occur during cable service in an operating power plant, but not in the sequential thermal and radiation stress commonly used to simulate aging in the laboratory, then the aging case used in qualification may not be sufficiently conservative to envelope service aging.

In this report, the effect of order of exposure to thermal and gamma radiation stress on two common cable insulation materials used in nuclear containment—cross-linked polyethylene (XLPE) and ethylene-propylene-diene elastomer (EPDM)—was directly investigated. Accelerated aging experiments were conducted at constant gamma dose rate and temperature at a series of exposure times to understand cable degradation dependence on the sequence of the applied stresses. The dose rate, total doses, and temperature used were selected based on input from expert stakeholders and on experimental resource constraints. Characterization methods including mass change, tensile elongation at break, carbonyl index, total color difference, density, indenter modulus, and indentation relaxation constant were employed to quantify the severity of three selected aging scenarios: (1) simultaneous [*T/R*, thermal and irradiation], (2) sequential [*T+R*, thermal followed by irradiation], and (3) sequential [*R+T*, irradiation followed by thermal].

The characterization results yielded insights into lifetime prediction of low-voltage nuclear instrumentation cables. Most significantly, sequential aging was found to produce a significantly different operational lifetime (defined here as time to 50% of the unaged specimen elongation at break) when compared to simultaneous aging depending on the insulating material type and aging scenario. For XLPE, lifetimes were found to be less for the sequential thermal followed by irradiation aging than for the simultaneous aging scenario, but greater for the sequential irradiation followed by thermal aging scenario. Conversely, for EPDM, performance lifetimes were found to be less for the sequential irradiation followed by thermal aging than for the simultaneous aging scenario, but greater for the sequential thermal followed by irradiation aging scenario. Overall conclusions for the materials and conditions investigated here are that 1) the relative severity of simultaneous versus sequential exposure to elevated temperature and gamma radiation varies with cable insulation material, and that 2) simultaneous exposure, as anticipated during in-plant cable service, is not always more severe than sequential exposure, commonly used in electrical cable qualification. These results seem to imply that qualification based on sequential exposure is not necessarily less conservative than if it were based on simultaneous exposure.

This report also demonstrates that mass change may be a useful technique for estimating the degradation of cables insulated with EPDM, particularly with the simultaneous and sequential irradiation followed by thermal aging scenarios, because a sharp decrease in mass was observed to correlate to a reduction in tensile elongation at break. In addition, the total color difference was observed to be a possibly advantageous non-destructive characterization method to estimate cable insulation lifetime as the technique is sensitive to cable insulation degradation and principal component analysis demonstrated a strong correlation between total color difference and elongation at break. Lastly, principal component analysis was found to be a promising approach to quantify the correlation between different characterization techniques for cable insulation lifetime.

Understanding material-specific aging mechanisms, differences between laboratory accelerated aging and in-plant service aging and identifying the most effective methods for non-destructively tracking aging are important for long-term nuclear power plant operation. This knowledge can guide cable aging management programs and re-licensing activities by prioritizing cable replacement decisions for cost-effective, efficient, and safe operation.

ACKNOWLEDGEMENTS

This work was sponsored by the U.S. Department of Energy, Office of Nuclear Energy, for the Light Water Reactor Sustainability (LWRS) Program Materials Research Pathway. The authors extend their appreciation to Pathway Lead Dr. Thomas Rosseel for LWRS programmatic support and Stephen Taylor for assistance with data collection. This work was performed at the Pacific Northwest National Laboratory (PNNL). PNNL is operated by Battelle for the U.S. Department of Energy under contract DE-AC05-76RL01830.

CONTENTS

SUMMARY iv

ACKNOWLEDGEMENTS v

CONTENTS vi

FIGURES vii

TABLES ix

ACRONYMS x

1. INTRODUCTION 1

2. MATERIALS 2

3. SIMULTANEOUS AND SEQUENTIAL THERMAL/GAMMA AGING 5

4. EXPERIMENTAL METHODS 7
   - 4.1 Mass Measurement Using an Analytical Balance 7
   - 4.2 Elongation at Break Measurement Using Video Extensometry 7
   - 4.3 Carbonyl Index Measurement Using FTIR 10
   - 4.4 Total Color Difference Measurement Using a Digital Camera 11
   - 4.5 Density Measurement Using Archimedes' Principle 12
   - 4.6 Indenter Modulus and Relaxation Constant Measurement 13

5. POLYMER DEGRADATION THEORY 15
   - 5.1 First-Order Reaction Kinetics 15
   - 5.2 Deviation from First-Order Reaction Kinetics 16
   - 5.3 Principal Component Analysis 18

6. RESULTS OF SIMULTANEOUS VERSUS SEQUENTIAL AGING CHARACTERIZATION 20
   - 6.1 Mass Change 20
   - 6.2 Elongation at Break 23
   - 6.3 Carbonyl Index 24
   - 6.4 Total Color Difference 28
   - 6.5 Indenter Modulus and Relaxation Constant 30

7. DISCUSSION OF CHARACTERIZATION RESULTS 33
   - 7.1 Mechanisms of Polymer Degradation 33
   - 7.2 Principal Component Analysis of the Aging Scenarios 35
   - 7.3 Sensitive Measures of Aging 36
   - 7.4 Comparison to Previous Work 38

8. CONCLUSIONS 39

9. REFERENCES 40

FIGURES

Figure 1. Exposed conductors within an exemplary low-voltage nuclear grade instrumentation cable. 3

Figure 2. FTIR absorbance spectrum of the white as-received (left) XLPE and (right) EPDM low-voltage nuclear grade cable insulation. 4

Figure 3. Extracted, labeled, and clipped insulation specimens prior to aging. 5

Figure 4. Clipped insulation specimens hung in the oven located at the HEF facility. 6

Figure 5. Fisher Scientific ALF104 analytical balance used to measure insulation mass. 7

Figure 6. A) Testing schematic for video extensometry of the insulation specimens and digital images of the B) test frame and C) digital camera positioning. 8

Figure 7. Process for analyzing insulation specimens using video extensometry. 9

Figure 8. Thermo Scientific Nicolet iS10 FTIR with ATR adapter used to measure carbonyl index. 10

Figure 9. Example (left) FTIR spectrum for EPDM insulation demonstrating the measurement methodology and (right) PCA loadings in the carbonyl region showing highest weighting (variations) at a wavenumber of approximately 1715 cm^{-1} (see Section 5.3 for more information). 10

Figure 10. Digital camera and light booth orientation for total color difference image collection. 11

Figure 11. Conversion of the A) input color image to a B) multispectral calibrated image. 12

Figure 12. Sartorius CPA225D analytical balance used to measure insulation density. 13

Figure 13. A) Indenter Polymer Aging Monitor and B) pocket PC used for data collection. 14

Figure 14. Example plots demonstrating the A) indenter modulus and B) relaxation constant measurement methodology. 14

Figure 15. Proposed mechanisms for radiation-to-thermal sequential aging by Gillen et al. [40]. 16

Figure 16. The average Δm of the (left) XLPE and (right) EPDM insulation specimens after aging. *T* represents thermal aging only (150°C) and *R* represents radiation aging at room temperature (26°C, 300 Gy/hr). The solid and dashed lines represent fitting of the data for two insulation specimens to the model in Equation (11) using the parameters of Table 6. 21

Figure 17. The average Δm due to irradiation (300 Gy/hr) after thermal aging (150°C) for (top) XLPE and (bottom) EPDM. 22

Figure 18. The average Δm due to heating (150°C) after irradiation (300 Gy/hr) for (top) XLPE and (bottom) EPDM. 23

Figure 19. The averaged and normalized EAB analyzed using video extensometry for the aged (left) XLPE and (right) EPDM insulation specimens. The solid lines represent fitting of the data to the model in Equation (11) using the parameters of Table 7. 24

Figure 20. FTIR absorbance spectra for the XLPE insulation specimens. The carbonyl (1715 cm^{-1}) and methylene (2848 cm^{-1}) peaks are indicated. 26

Figure 21. FTIR absorbance spectra for the EPDM insulation specimens. The carbonyl (1715 cm^{-1}) and methylene (2848 cm^{-1}) peaks are indicated. 27

Figure 22. The average CI of the (left) XLPE and (right) EPDM insulation specimens after aging. The solid lines represent fitting of the data to the model in Equation (11) using the parameters of Table 8. 28

Figure 23. Original color digital images of the (top) XLPE and (bottom) EPDM specimens for select exposures. 29

Figure 24. The average total color difference of the (left) XLPE and (right) EPDM insulation specimens after aging. 30

Figure 25. The average IM of the (left) XLPE and (right) EPDM insulation specimens after aging. The solid lines represent fitting of the data to the model in Equation (11) using the parameters of Table 9. 31

Figure 26. The average τ of the (left) XLPE and (right) EPDM insulation specimens after aging. The solid lines represent fitting of the data to the model in Equation (11) using the parameters of Table 10. 32

Figure 27. The average density of the (left) XLPE and (right) EPDM insulation specimens after aging. The solid lines represent fitting of the data to the model in Equation (11) using the parameters of Table 11. 34

Figure 28. Variable correlation plot of PCA for the methods of Section 6 for (left) XLPE and (right) EPDM. 36

Figure 29. Score plot for PCA of the aging scenarios for (left) XLPE and (right) EPDM. The direction of increasing exposure is indicated on the plots and the unaged specimens are shown as +. 36

Figure 30. Normalized variations in the measured properties for aged insulation specimens: (left) XLPE and (right) EPDM. 37

TABLES

Table 1. The most common nuclear cable insulation and jacket material types within containment [3]; values shown are approximations. 2

Table 2. The nuclear grade instrumentation cables used in this study. 2

Table 3. Evaluated test conditions for sequential versus simultaneous exposure of nuclear grade XLPE and EPDM insulation cable. 6

Table 4. Test parameters for EAB measurement. 8

Table 5. The linear slope in Δm after initial exposure (3 days); a second linear slope was observed for EPDM with the *T/R* and *R+T* aging scenarios after 23 days and 36 days of exposure, respectively. 20

Table 6. Evaluated model parameters for Δm using Equation (11). Fitting was conducted for two insulation specimens using MATLAB® curve fitting software to minimize the sum of squares of the residuals. 20

Table 7. Evaluated model parameters for EAB using Equation (11) and the estimated critical time, t_c. Fitting was conducted using MATLAB® curve fitting software to minimize the sum of squares of the residuals. 24

Table 8. Evaluated model parameters for CI using Equation (11). Fitting was conducted using MATLAB® curve fitting software to minimize the sum of squares of the residuals. 28

Table 9. Evaluated model parameters for IM using Equation (11). Fitting was conducted using MATLAB® curve fitting software to minimize the sum of squares of the residuals. 31

Table 10. Evaluated model parameters for τ using Equation (11). Fitting was conducted using MATLAB® curve fitting software to minimize the sum of squares of the residuals. 32

Table 11. Evaluated model parameters for density using Equation (11). Fitting was conducted using MATLAB® curve fitting software to minimize the sum of squares of the residuals. 34

Table 12. Lifetime prediction of sequential aging scenarios normalized to the simultaneous aging scenario. 38

Table 13. Previous work, with sequential aging normalized to the simultaneous aging scenario (*T/R*) [3]. 38

ACRONYMS

ASTM	ASTM International
ATR	attenuated total reflectance
CI	carbonyl index
CIE	Commission on Illumination
CPE	chlorinated polyethylene elastomer
CSPE	chlorosulfonated polyethylene
DLO	diffusion limited oxidation
EAB	elongation at break
EPDM	ethylene-propylene-diene elastomer
EPR	ethylene-propylene rubber
ETFE	ethylene tetrafluroethylene
EMDA	Expanded Materials Degradation Assessment [1]
FTIR	Fourier-transform infrared spectroscopy
HEF	High Exposure Facility
IEC	International Electrotechnical Commission
IEEE	Institute of Electrical and Electronics Engineers
IM	indenter modulus
ISO	International Standards Organization
LWRS	Light Water Reactor Sustainability
NPP	nuclear power plant
NIH	National Institute of Health
ODE	ordinary differential equation
OIT	oxidation induction time
PC	principal component
PC1	principal component 1 (containing the most variability)
PC2	principal component 2 (containing the second most variability)
PCA	principal component analysis
PE	polyethylene
PNNL	Pacific Northwest National Laboratory
PVC	polyvinyl chloride
R	radiation-only aging
R+T	sequential aging (irradiation followed by thermal)
ROI	region of interest

SR	silicone rubber
sRGB	standard red-green-blue
T	temperature-only aging
T+R	sequential aging (thermal followed by irradiation)
T/R	simultaneous aging (thermal and irradiation)
XLPE	cross-linked polyethylene
XLPO	cross-linked polyolefin
τ	relaxation constant

1. INTRODUCTION

Approximately 20% of the electricity produced in the United States comes from nuclear power plants (NPPs) [2]. Originally, NPPs were qualified for an operational lifetime of 40 years [3,4]. As described in the foreword of the U.S. Nuclear Regulatory Commission's (NRC's) Expanded Materials Degradation Assessment (EMDA) Volume 5: Aging of Cables and Cable Systems [5], and according to Title 10 of the Code of Federal Regulations, Part 54 (10 CFR 54), Requirements for Renewal of Operating Licenses for Nuclear Power Plants, NPPs can apply for 20-year license extensions following the original 40-year operating period. While most NPPs have entered extended lifetimes of up to 60 years, some are considering license extension for up to 80 years of operational lifetime [6]. The viability of a second license renewal is dependent upon the NPPs operating safely in accordance with the licensing basis established with the original 40-year license. Hence, the NRC has developed aging management program requirements to promote the safe function of NPPs over license extension periods. The EMDA report identified cable aging-related issues that may be important for the second license renewal of NPPs.

Based upon the issues raised in EMDA Volume 5, a U.S. Department of Energy-sponsored research and development roadmap workshop report [7], and additional emerging issues, Pacific Northwest National Laboratory (PNNL) prioritized a list of 11 cable-aging knowledge gaps focusing on the degradation of cable insulation [8]. From this list, four knowledge gaps were selected for investigation as described by Fifield et al. [8], including: (1) diffusion limited oxidation (DLO) effects due to oxygen permeability hindrance at the polymer surface during accelerated aging [9,10], (2) dose-rate effects where polymer degradation is not only a function of total absorbed gamma dose, but also of the dose rate [11], (3) inverse temperature effects in which degradation due to gamma irradiation is higher at lower temperatures [12], and (4) synergistic effects due to the combined interactions between temperature and radiation [13,14]. Of these four cable knowledge gaps, the focus of this report is on the "synergistic effects."

Arguably, synergistic effects are the least well understood cable knowledge gap [15] because the interactions between temperature and radiation are not additive, but coupled. To better understand synergistic effects, Ito modified the Arrhenius equation by correlating the first-order rate constant as the superposition of rate constants due to temperature, radiation, and a coupling between temperature and radiation [16]. More recent work by Gillen extended this approach to systems with non-first-order behavior, a set that includes most materials [13]. However, even using these approaches, estimation of the rate constant, which is necessary to predict cable insulation lifetimes in synergistic aging scenarios, is difficult because the stress order also influences the rate constant. Because initial qualification of NPP cable insulation was historically conducted using a sequential aging scenario (e.g., thermal aging followed by irradiation), instead of the simultaneous aging scenario likely characteristic of actual service aging (thermal aging combined with irradiation), there are uncertainties regarding how conservative these accelerated aging tests were [17].

In this report, two common nuclear cable insulation materials [3]—cross-linked polyethylene and ethylene-propylene-diene elastomer—were aged simultaneously and sequentially at a constant dose rate and temperature to evaluate the effects of the applied stress sequence [8]. A variety of characterization techniques were employed to assess the aging scenarios and to supply more complete information to regulators, operators, and other decision-makers about the long-term operation of nuclear cables exposed to synergistic effects. First, in Section 2, the two cable insulation materials investigated are described. Then, in Section 3, accelerated aging involving elevated temperature and gamma radiation applied to the insulation specimens is described. In Section 4, information is provided about the methods used to characterize changes in the insulation materials upon aging, including mass change, tensile elongation at break, carbonyl index, total color difference, density, indenter modulus, and relaxation constant. Section 5 discusses the theory of polymer degradation related to the conditions employed. Characterization results are provided in Section 6, followed by a discussion of results in Section 7. Finally, concluding remarks are made in Section 8.

2. MATERIALS

To elevate the relevance of this work, the materials investigated were selected from those commonly found within nuclear containment [3]. Both cross-linked polyethylene (XLPE) and ethylene-propylene-diene elastomer (EPDM)[1] were selected for analysis of the order of sequence and synergistic effects because insulation material types similar to these are present within at least 75% of nuclear containments in U.S. NPPs, as shown in Table 1. In addition to the selected material type, low-voltage nuclear grade instrumentation cables were selected because approximately 81% of electrical cables within U.S. NPPs are low-voltage instrument and control cables [18]. Manufacturer information for the selected cables is shown in Table 2.

Table 1. The most common nuclear cable insulation and jacket material types within containment [3]; values shown are approximations.

Material	Percent of Units (%)
XLPE	90
EPDM/EPR	75
SR	27
CSPE	24
ETFE	15
PVC	7
PE	3
Neoprene	3
Polyimide	3
Polyalkene	2

XLPE = cross-linked polyethylene; EPDM = ethylene-propylene-diene elastomer; EPR = ethylene-propylene rubber; SR = silicone rubber; CSPE = chlorosulfonated polyethylene; ETFE = ethylene tetrafluoroethylene; PVC = polyvinyl chloride; PE = polyethylene.

Table 2. The nuclear grade instrumentation cables used in this study.

Manufacturer	Product Identifier	Sourced From	Jacket Material	Insulation Material
RSCC Wire & Cable	I46-0021	Manufacturer	CSPE	XLPE
Samuel Moore Group	Dekoron® 2/C 16 AWG 600 V	Electric Power Research Institute (EPRI)	CSPE	EPDM

CSPE = chlorosulfonated polyethylene; XLPE = cross-linked polyethylene; EPDM = ethylene-propylene-diene elastomer; AWG = American Wire Gauge.

An example of the components of a low-voltage nuclear grade instrumentation cable are shown in Figure 1. For the selected material types, both the insulation without the conductor and the insulation with the conductor intact were analyzed for specific characterization methods as discussed in Section 4. The white insulation was extracted from the electrical instrumentation cables of Table 2 by first carefully

[1] In EPDM, E refers to ethylene, P to propylene, D to diene, and M to classification of the material as a rubber "having a saturated chain of the polymethylene type" in ASTM D1418 [19]. (The Vanderbilt Rubber Handbook, 14th Edition. Edited by Martin F. Sheridan. 2010 [20]).

removing the chlorosulfonated polyethylene (CSPE) jackets. For the insulation specimens without a conductor, a wire stripping tool was used to score the insulation in 100 mm increments. Afterwards, the exposed conductors were fixed in place with a vice and the insulation was removed by gently pulling the insulation from over the conductors. The extracted insulation was 100 mm in length. For the insulation specimens with a conductor, specimens were cut to 50 mm length. The tubular cross-sections of the insulation were measured as 4.74 mm^2 (1.28 ± 0.04 mm inner diameter and 2.79 ± 0.08 mm outer diameter) and 4.64 mm^2 (1.35 ± 0.07 mm inner diameter and 2.78 ± 0.04 mm outer diameter) for the XLPE and EPDM insulations, respectively.

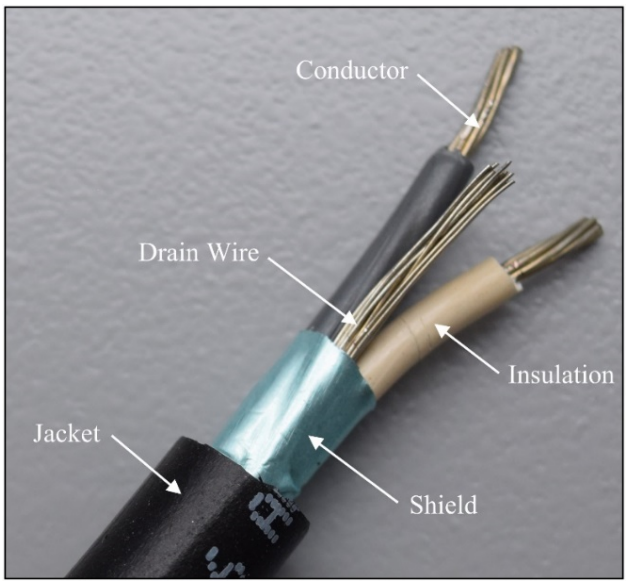

Figure 1. Exposed conductors within an exemplary low-voltage nuclear grade instrumentation cable.

The material types of the extracted insulation were confirmed by comparing their absorbance spectra to literature data using Fourier-transform infrared spectroscopy (FTIR). The spectra of the as-received, or unaged, insulation specimens are shown in Figure 2. Due to their chemical structure, methylene absorption (-CH_2-) is useful for identification of both XLPE and EPDM. For both material types, strong characteristic methylene asymmetric and symmetric stretching absorbance peaks were measured at 2916 cm^{-1} and 2848 cm^{-1}, respectively [21,22]. In addition, both material types demonstrate characteristic methylene bending modes at 1462 cm^{-1} (scissoring), 1349 cm^{-1} (wagging), and 729 cm^{-1} (rocking), similar to those reported in literature [23–25]. Absorption was observed for the unaged EPDM specimen at 1050 cm^{-1}, likely due to trans hydrogen atoms on a double bond—an artifact of the vulcanization process [26]. Furthermore, absorption of trans-substituted [27] and tri-substituted [28] alkenes were found at 866 cm^{-1} and 808 cm^{-1} for the unaged EPDM specimen, respectively. Both material types produced weak carbonyl bonds in the range of 1600 to 1720 cm^{-1}, likely due to oxidation.

Location	K (cm^{-1})	Functional Groups
(1)	2916	CH_2 asymmetric stretch
(2)	2848	CH_2 symmetric stretch
(3)	1720	C=O stretch
(4)	1462	CH_2 scissoring
(5)	1349	CH_2 wagging
(6)	1050	Trans hydrogen
(7)	866	Trans-substituted alkene
(8)	808	Tri-substituted alkene
(9)	729	CH_2 rocking

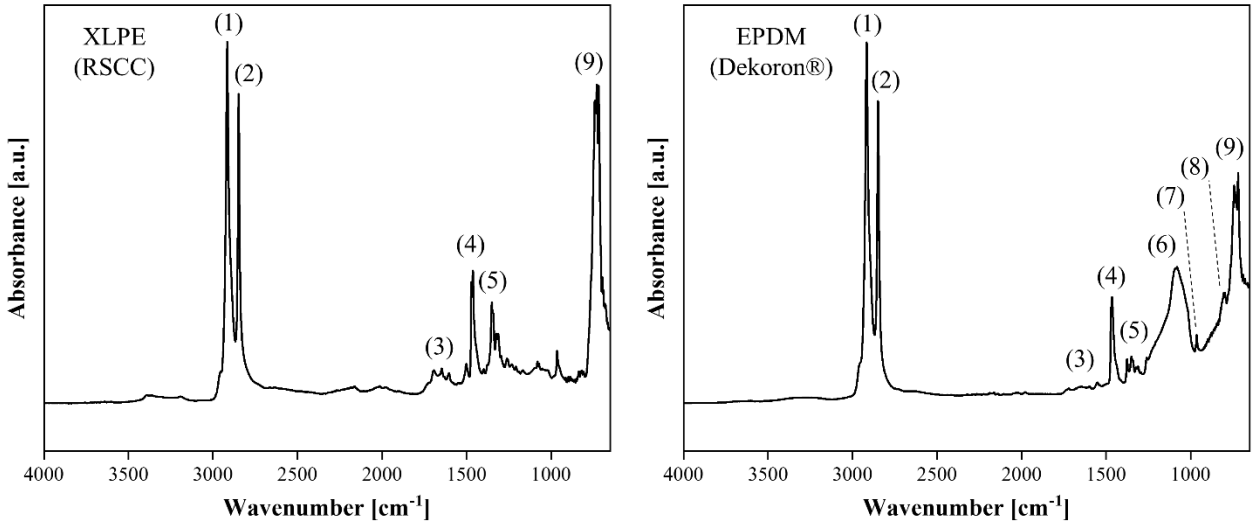

Figure 2. FTIR absorbance spectrum of the white as-received (left) XLPE and (right) EPDM low-voltage nuclear grade cable insulation.

3. SIMULTANEOUS AND SEQUENTIAL THERMAL/GAMMA AGING

Prior to aging, the mass of each specimen was measured. Each specimen was then attached to a clip labeled with a unique specimen identifier, as shown in Figure 3. Afterwards, the specimens were hung from a rack and exposed to one of three aging scenarios:

1. *T/R*: simultaneous heating at 150°C and gamma irradiation at 300 Gy/hr;
2. *T+R*: heating at 150°C for a designated duration followed by gamma irradiation at 300 Gy/hr for the same duration;
3. *R+T*: irradiation at 300 Gy/hr without heating for a designated duration followed by heating at 150°C for the same duration.

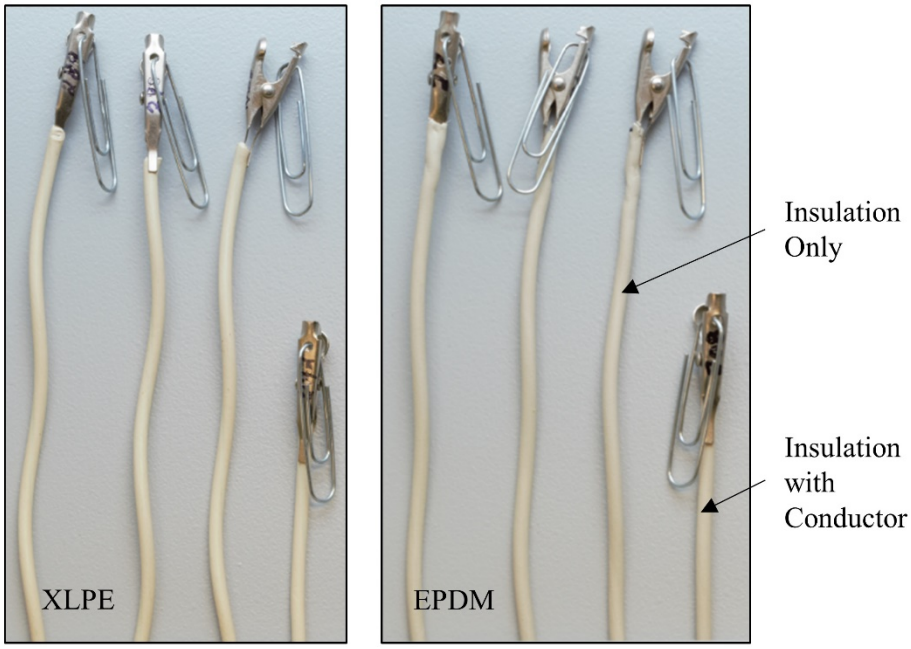

Figure 3. Extracted, labeled, and clipped insulation specimens prior to aging.

To evaluate the effects of the order of sequence on insulation degradation, the dose rate, total dose, and the temperature were held constant for each aging scenario and test condition. Using an approximately 11,000 Ci Cobalt-60 (Co-60) source, gamma irradiation was conducted at the High Exposure Facility (HEF) at PNNL. The dose rate was held constant by positioning the specimens at approximately 56 cm from the Co-60 source. The temperature was controlled through integrated thermocouple feedback and provided by a mechanical convection oven, as shown in Figure 4; the oven was modified to enable the heating elements to be independent of the oven fans to maintain air circulation in the absence of heating. With no heating, the oven was at an ambient temperature of 26°C. The test conditions for each aging scenario described above are shown in Table 3. The 150°C temperature and 300 Gy/hr dose rate were selected based on time constraints for the exposure experiment to achieve the radiation exposure of all three aging scenarios (*T/R*, *T+R*, and *R+T*) within the approximately 120 days of irradiation time available for the particular campaign at the HEF. It is acknowledged that DLO is likely to occur to some extent at temperatures above 130°C and at dose rates above 100 Gy/hr, but the complicating effects of DLO are not considered here. Unaged specimens were evaluated for benchmark reference.

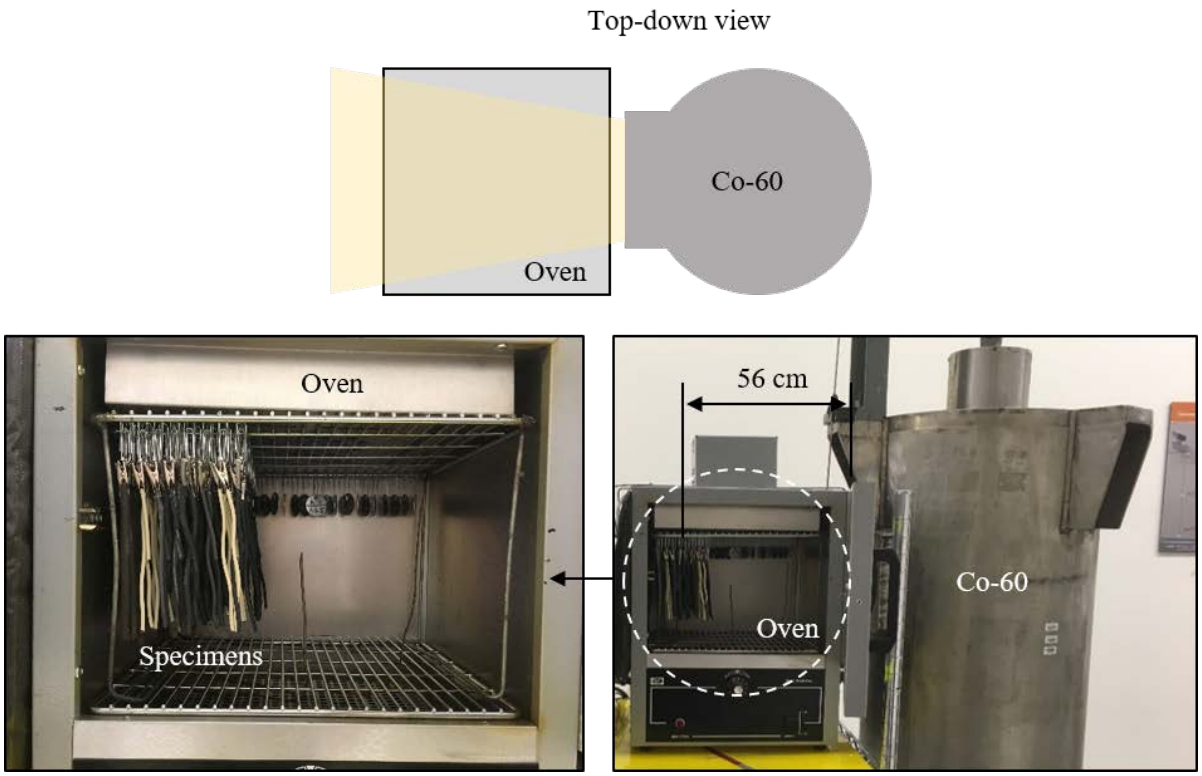

Figure 4. Clipped insulation specimens hung in the oven located at the HEF facility.

Table 3. Evaluated test conditions for sequential versus simultaneous exposure of nuclear grade XLPE and EPDM insulation cable.

Test Condition	Dose (kGy)	Exposure (Days)
1	Unaged	
2	20	3
3	40	5
4	60	9
5	150	21
6	170	23
7	260	36
8	280	39
9	300	41
10	320	44

4. EXPERIMENTAL METHODS

To investigate the effects of simultaneous (*T/R*) aging, in comparison to sequential aging (*T+R*, *R+T*), on the degradation behavior of the insulation specimens, seven different characterization methods were employed as discussed below.

4.1 Mass Measurement Using an Analytical Balance

An analytical balance (Fisher Scientific ALF104, ± 0.001 g resolution, see Figure 5) was used to measure the mass of the insulation specimens before and after aging. In addition, the mass was measured after the first aging cycle for the sequential aging scenarios (after thermal for *T+R* and after radiation for *R+T*). The mass of three insulation specimens was measured for each aging condition for the insulation specimens with no conductor.

Figure 5. Fisher Scientific ALF104 analytical balance used to measure insulation mass.

4.2 Elongation at Break Measurement Using Video Extensometry

Following IEC/IEEE 62582-3, the tensile elongation at break (EAB) was measured for the aged insulation specimens with no conductor. Table 4 lists the test parameters for both material types. For each aging condition, the insulation specimens were cut to a length of 45 mm and the inner and outer diameters were measured using a digital caliper. A black permanent marker with a fine tip size was used to draw two gauge marks centered and at 20 mm separation on the insulation specimens. Afterwards, the insulation specimens were conditioned following ASTM D618 Procedure A: at least 40 hours at 23°C ± 2°C and 50% ± 10% relative humidity. The humidity was controlled by placing the specimens in a covered desiccator charged with a saturated solution of potassium carbonate and deionized water (fixed humidity point of 43% [29]). A data logger (Omega OM-EL-USB-2-LCD-PLUS) was placed in the desiccator to monitor both the temperature and humidity. After conditioning, end tabs of 5 mm length were gently slipped over the ends of the specimens with an approximate gap of 2 mm between the ends of the specimens and the end tabs (see Figure 6A). The method of attachment of the end tabs to the specimen depended upon the material type: the end tabs were gently compressed prior to placement on the XLPE specimens and two layers of tissue (Kimtech Science Kimwipes) were placed between the specimen and end tabs to avoid slippage of the end tabs on the EPDM specimens. After attachment of the end tabs, the specimens were placed centered and along the axis of a pair of pneumatic grips at a separation of 30 mm. A testing rate lower than that specified in IEC/IEEE 62582-3 was incorporated to avoid early failure of the specimens. As shown in Figure 6B, a tensile testing machine (Instron® 3360 Universal Testing System, Norwood, MA) was used to apply tension to the specimens. For each aging condition, EAB was measured for four insulation specimens.

Table 4. Test parameters for EAB measurement.

Material Type	Test Rate (mm/min)	End Tab Material	Grip Pressure (psi)
XLPE (RSCC)	10	XLPE (Grainger, 10A671)	60
EPDM (Dekoron®)	20	CSPE (RSCC, I46-0021 Jacket)	40

CSPE = chlorosulfonated polyethylene; EPDM = ethylene-propylene-diene elastomer; XLPE = cross-linked polyethylene.

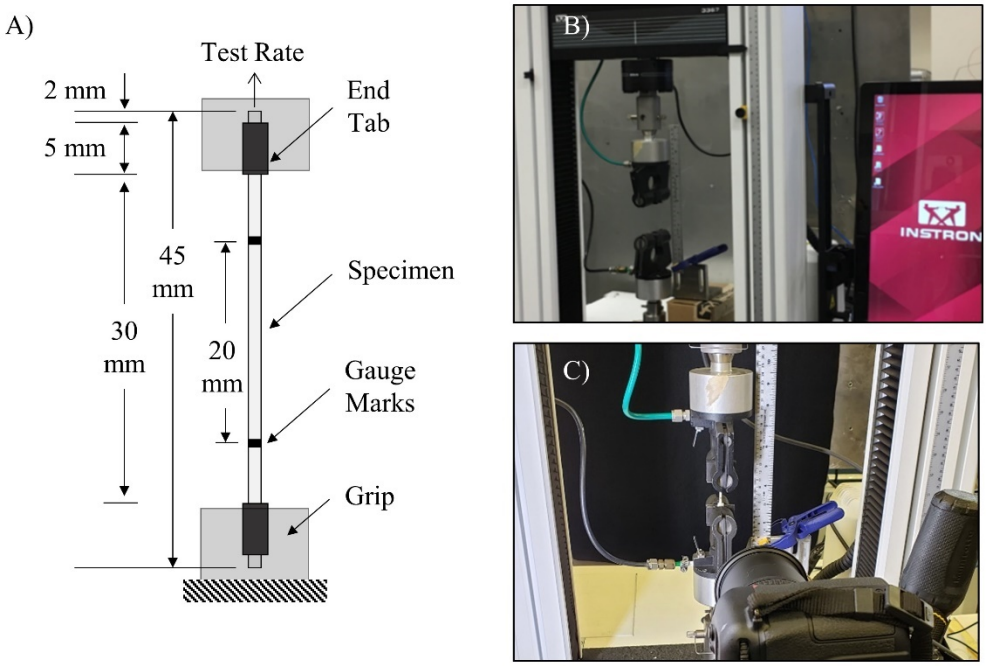

Figure 6. A) Testing schematic for video extensometry of the insulation specimens and digital images of the B) test frame and C) digital camera positioning.

For each aging condition, the tensile test was video recorded. As shown in Figure 6C, a tripod was used to mount and orient a digital camera (Nikon D7500) such that the entire extension of the specimens could be captured. The settings of the digital camera were optimized to enhance video extensometry processing: 1080p resolution to reduce file size, 1/250 s exposure time to ensure clean break frame detection, an aperture of f10 to enhance the depth of field, and an ISO setting of 1000 to balance specimen illumination and background noise. Specimen lighting was controlled by placing two light sources (Genaray SP-S-1000D, 100% illumination) behind and to either side of the camera and directing the light towards the specimens. In addition, edge detection during video processing was enhanced by the placement of a diffuse black background behind the specimens. Video recording was started prior to elongation of the specimen and stopped immediately upon failure of the specimen.

After video recording, each video was processed using an in-house-developed video extensometry code written in MATLAB® (MathWorks®, Natick, MA) and R (The R Foundation, r-project.org). The videos were analyzed following the process shown in Figure 7. The elongation (%) [30] was calculated for each frame as shown in Equation (1), where E_0 and E_c are the starting and current gauge length (based on pixel location), respectively. The final elongation measured was recorded as the EAB.

$$e = 100\frac{E_c - E_0}{E_0} \quad (1)$$

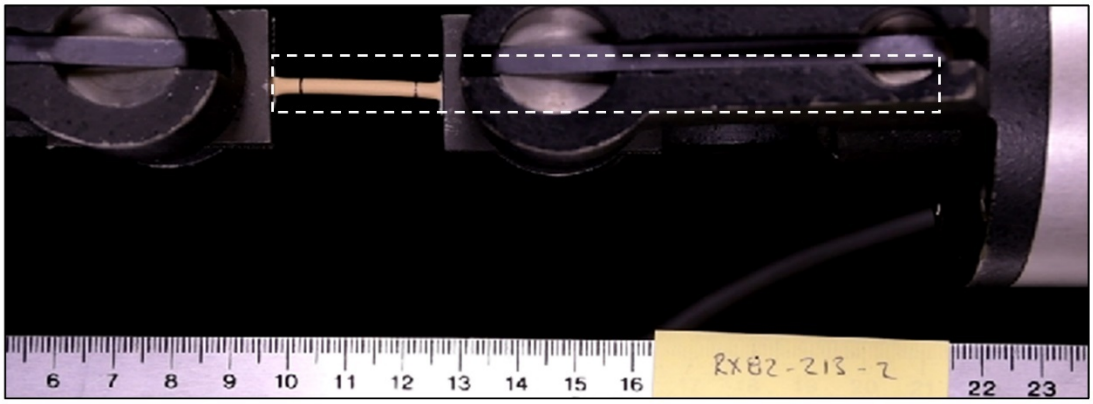

A) Example output frame from the digital camera during specimen elongation.

B) Frames were cropped (--- line shown above), converted to greyscale, and thresholding was applied (pixels < 25 set to 25).

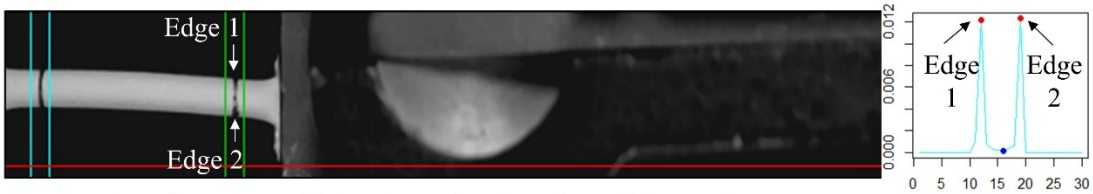

C) Edge detection was applied to determine the edges of the specimens.

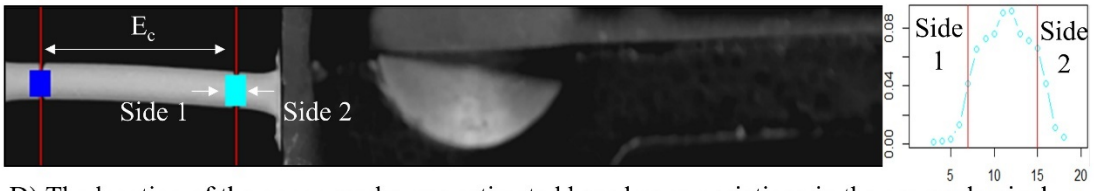

D) The location of the gauge marks was estimated based upon variations in the greyscale pixel intensity. The distance between gauge marks (in pixels) was stored for each frame.

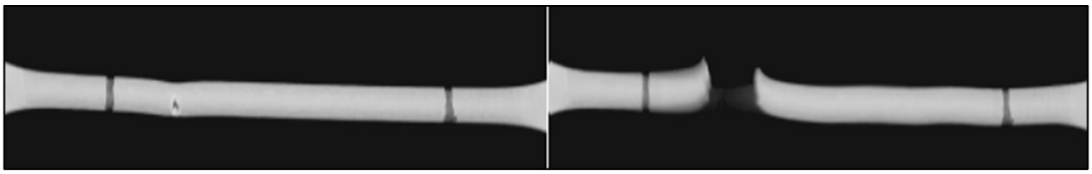

E) A frame-to-frame increase in the gauge length by more than 15 pixels was specified as the break frame.

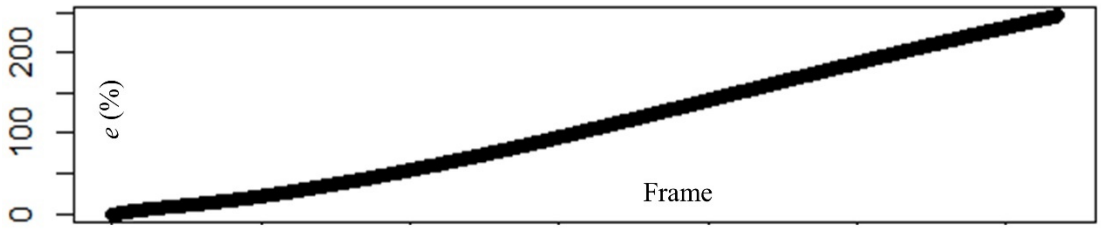

F) For each frame the elongation was measured. After specimen failure, the elongation curve was smoothed using locally weighted scatterplot smoothing.

Figure 7. Process for analyzing insulation specimens using video extensometry.

4.3 Carbonyl Index Measurement Using FTIR

FTIR attenuated total reflectance (ATR) (Thermo Scientific Nicolet iS10) was used to measure the carbonyl index at the external surface of the aged insulation specimens with no conductor. Approximately 5 mm was extracted from the end of each insulation specimen for FTIR analysis. Specimen surfaces were gently cleaned with deionized water after aging to minimize surface contamination because FTIR ATR is a surface sensitive technique (for example, penetration depths are typically on the order of 4 µm at 500 cm^{-1} and 0.5 µm at 4000 cm^{-1} for XLPE and a diamond ATR crystal [31]). After cleaning, the specimens were conditioned following the same procedure as described in Section 4.2 (at least 40 hours at 23°C ± 2°C and 50% ± 10% relative humidity). A background spectrum was collected prior to measurement for spectra subtraction. To enhance the measured absorbance values, an anvil tool was used to compress the specimens against the diamond ATR crystal to ensure complete contact, see Figure 8. A total of 64 scans were collected for each measurement to reduce background noise. In addition, spectra were collected at two locations on each specimen surface to account for variations based upon measurement location and two specimens were evaluated for each aging condition (a total of four measurements for each aging condition).

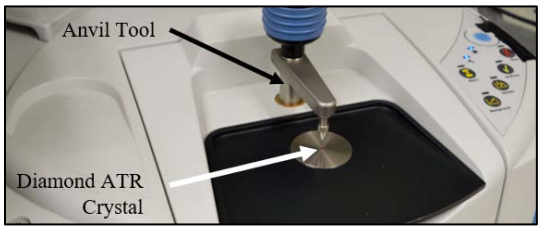

Figure 8. Thermo Scientific Nicolet iS10 FTIR with ATR adapter used to measure carbonyl index.

Analysis of the spectra peaks was conducted using R (The R Foundation, r-project.org). Peak absorbance intensities corresponding to the methylene group (maximum absorbance between 2846 cm^{-1} and 2850 cm^{-1}, CH_2 symmetric stretching [32]) and carbonyl group (1715 cm^{-1}, C=O stretch [33]) were recorded from a baseline (2000 cm^{-1}) as shown in Figure 9. The evaluated wavenumber associated with the carbonyl group (1715 cm^{-1}) was confirmed through principal component analysis (PCA, see Section 5.3) to provide the largest weighting between 1600 cm^{-1} and 1800 cm^{-1}. The carbonyl index (CI) is given in Equation (2), where H_{2848} and H_{1715} are the peak absorbance intensities for the methylene and carbonyl groups, respectively.

$$CI = \frac{H_{1715}}{H_{2848}} \tag{2}$$

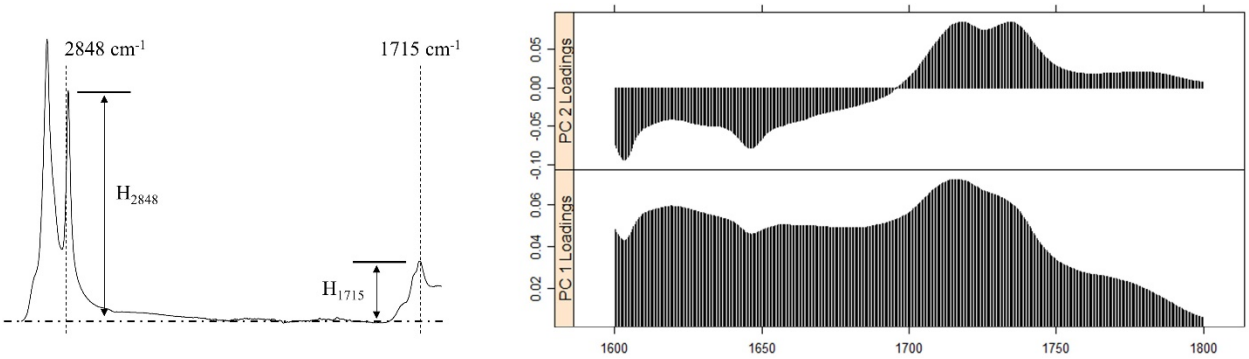

Figure 9. Example (left) FTIR spectrum for EPDM insulation demonstrating the measurement methodology and (right) PCA loadings in the carbonyl region showing highest weighting (variations) at a wavenumber of approximately 1715 cm^{-1} (see Section 5.3 for more information).

4.4 Total Color Difference Measurement Using a Digital Camera

Polymeric specimens darken upon aging when exposed to thermal and radiation stresses. Following ASTM D1729 and ASTM D2244, the total color difference (ΔE^*_{ab}) of the aged with respect to the unaged insulation specimens without a conductor was measured using a light booth (GTI MiniMatcher MM 2e) and digital camera (Nikon D5300). A clamp was used to fix the digital camera in place and orient the camera lens perpendicular to the display plane of the light booth (see Figure 10). To optimize the quality of the collected images, the digital camera settings were as follows: an exposure time of 1/3 s to enhance color saturation, an aperture of f14 to enhance depth of field, and an ISO setting of 100 to reduce background noise. A wireless remote control (Nikon ML-L3) was used to ensure the camera did not move during image collection and to facilitate batch processing. In the light booth, a standard International Commission on Illumination (CIE) D65 light was used; background lighting in the room was extinguished during image collection. To facilitate image calibration and conversion to the CIE XYZ color space (and subsequently the L*a*b* color space [defined below]), a color reference target was placed on the light booth display plane. The aged insulation specimens were placed next to the color reference target as shown in Figure 11A. Because of the issues with surface reflections on tubular specimens and variations in color along the specimen lengths, each insulation specimen was removed after image collection, rotated slightly, and then returned next to the color reference target before another image was captured. This process was repeated twice for a total of three images per insulation specimen and two insulation specimens were measured for each aging condition (a total of six images collected for each aging condition).

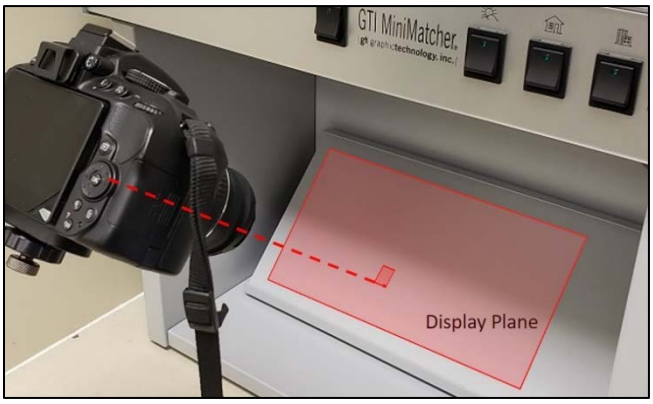

Figure 10. Digital camera and light booth orientation for total color difference image collection.

Due to their inherent components and internal processing, a digital camera and lens will modify the color in digital images; therefore, it is necessary to map these modified colors into a system with an absolute measure of color prior to quantifying color changes. ImageJ (NIH) was used in conjunction with the micaToolbox [34,35] to convert the collected images to the CIE XYZ color space. First, the six grey standards located on the bottom row of the color reference target (see Figure 11A) were converted to reflectance values using manufacturer-supplied standard Red Green Blue (sRGB) triplets for each grey standard and then using an iterative least log slope approach [36] to convert the triplets to reflectance values. Second, the grey reflectance values were used to create a linear normalized reflectance stack, or calibrated multispectral image, for each collected image. Third, regions of interest (ROIs) were manually specified for each calibrated image, as shown in Figure 11B. Care was taken to select regions with no reflections or shadows and a total of three ROIs were selected for each image for a total of eighteen data points for each aging condition. Fourth, a cone-catch model [35] was generated based upon the charted reflectance spectra of the color reference target. Fifth, the cone-catch model was used to map the linear normalized reflectance stack to the CIE XYZ color space and the XYZ color space values of the ROIs were measured. Lastly, the measured XYZ color space values were mapped to D65 reference white point CIE L*a*b* color space

through the built-in MATLAB® function *xyz2lab*. The total color difference is shown in Equation (3), where L^*_S, a^*_S, and b^*_S are the reference L*a*b* values and L^*_B, a^*_B, and b^*_B are the specimen L*a*b* values. The mean L*a*b values of the unaged specimens were selected as the reference values.

$$\Delta E^*_{ab} = \sqrt{(\Delta L^*)^2 + (\Delta a^*)^2 + (\Delta b^*)^2} \tag{3}$$

$$\Delta L^* = L^*_B - L^*_S$$

$$\Delta a^* = a^*_B - a^*_S$$

$$\Delta b^* = b^*_B - b^*_S$$

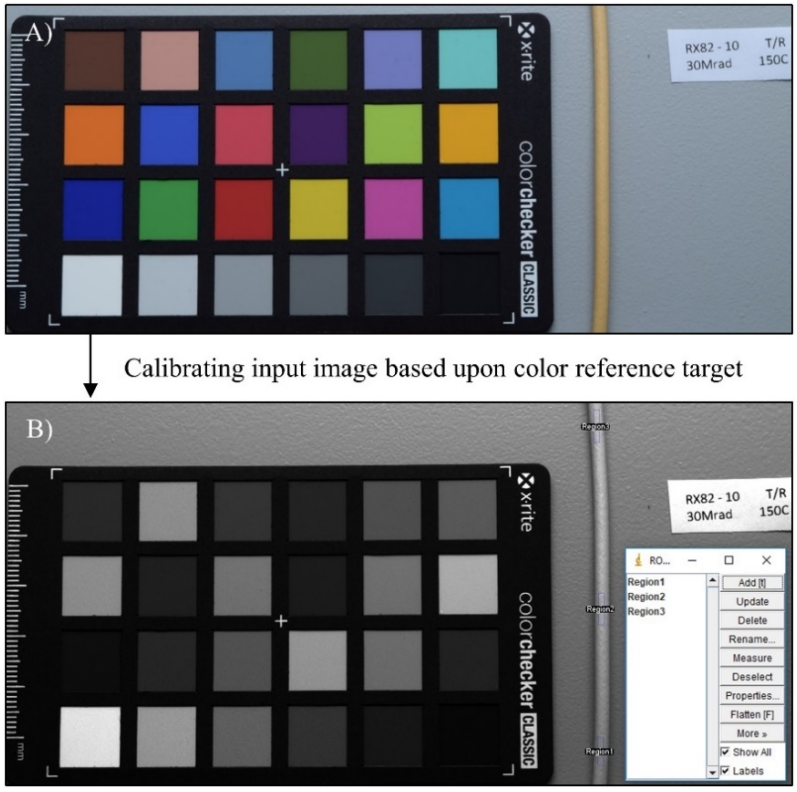

Figure 11. Conversion of the A) input color image to a B) multispectral calibrated image.

4.5 Density Measurement Using Archimedes' Principle

Following ASTM D792, the density of selected insulation specimens without conductor was measured. An approximate length of 5 mm was extracted from the end of the insulation specimens for density measurement. The specimens were conditioned following the same procedure described in Section 4.2 (at least 40 hours at 23°C ± 2°C and 50% ± 10% relative humidity). A high-resolution analytical balance (Sartorius CPA225D, ±0.0001 g) was used in conjunction with a density measurement kit (Sartorius YDK01) to measure the specimen mass in air and in water (see Figure 12). Prior to immersing the specimens, the mass of the specimens in air was measured. Afterwards, the specimens were wetted with isopropanol alcohol to limit the formation of air bubbles on the specimen surfaces. The specimens were then immediately placed in a convex sample holder immersed in deionized water (24.6°C ± 0.9°C); the sample holder was located at a depth of approximately 2.54 cm below the surface. The specimen apparent mass was then recorded, and the specimens were removed, again wetted with isopropanol, and set aside to

dry. The above process was repeated two times for a total of three sets of measurements per insulation specimen (a total of three measurements for each aging condition). The Archimedes' principle (water displacement) was used to determine the density (g/cm^3), as shown in Equation (4) [37], where m is the average mass in air (g), m_l is the average mass immersed in water (g), and ρ_l is the density of the liquid (g/cm^3) at the measurement temperature.

$$\rho = \frac{m\rho_l}{m - m_l} \tag{4}$$

Figure 12. Sartorius CPA225D analytical balance used to measure insulation density.

4.6 Indenter Modulus and Relaxation Constant Measurement

The indenter modulus (IM) of the aged insulation specimens with a conductor was measured following IEC/IEEE 62582-2. The specimens were conditioned following the same procedure as described in Section 4.2 (at least 40 hours at 23°C ± 2°C and 50% ± 10% relative humidity). After conditioning, the insulation specimens were placed within a cable clamp assembly of an Indenter Polymer Aging Monitor (AMS Corp. IPAM 4M, Tennessee, USA) as shown in Figure 13A. The insulation specimens were gently clamped within the IPAM to prevent displacement during measurement. An instrumented probe housed within the IPAM indented the external surface of the specimens at a loading rate of 5.1 mm/min and a maximum load of 8.9 N, similar to the recommendations of IEC/IEEE 62582-2. Each measurement was conducted under ambient laboratory conditions (approximately 21°C and 30% relative humidity). The indentation process was controlled, and data collected, through the usage of an external pocket PC (see Figure 13B). For each insulation specimen, a total of ten indentations were performed at three locations around the specimen circumference while avoiding indentation within 10 mm of each end of the specimen. Per IEC/IEEE 62582-2, the indenter modulus (N/mm) was calculated from the slope of the linear portion of the initial force versus deformation curve as shown in Figure 14A and Equation (5), where d_1 and d_2 are the displacements (mm) corresponding to force values of F_1 (1 N) and F_2 (4 N), respectively. In addition to the indenter modulus, the IPAM allows for easy measurement of the insulation specimen relaxation constant, τ. After the maximum load (8.9 N) has been reached during indentation, the probe stops moving and relaxation of the polymeric insulation was measured over time (see Figure 14B). The relaxation constant (s) is shown in Equation (6), where F_3 and F_4 are the force (N) values corresponding to measurement times of t_3 (2 s) and t_4 (3 s) after the probe has stopped moving, respectively. The average value and standard deviation of the indenter modulus and relaxation constant are reported after removing the highest and lowest measurement values due to differences in specimen construction, dimensions, and stabilization.

$$IM = \frac{F_2 - F_1}{d_2 - d_1} \quad (5)$$

$$\tau = \left| \frac{t_4 - t_3}{ln\left(F_4/F_3\right)} \right| \quad (6)$$

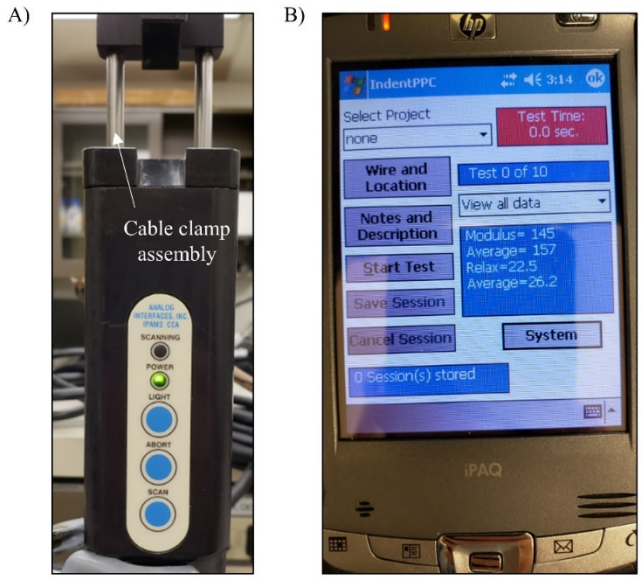

Figure 13. A) Indenter Polymer Aging Monitor and B) pocket PC used for data collection.

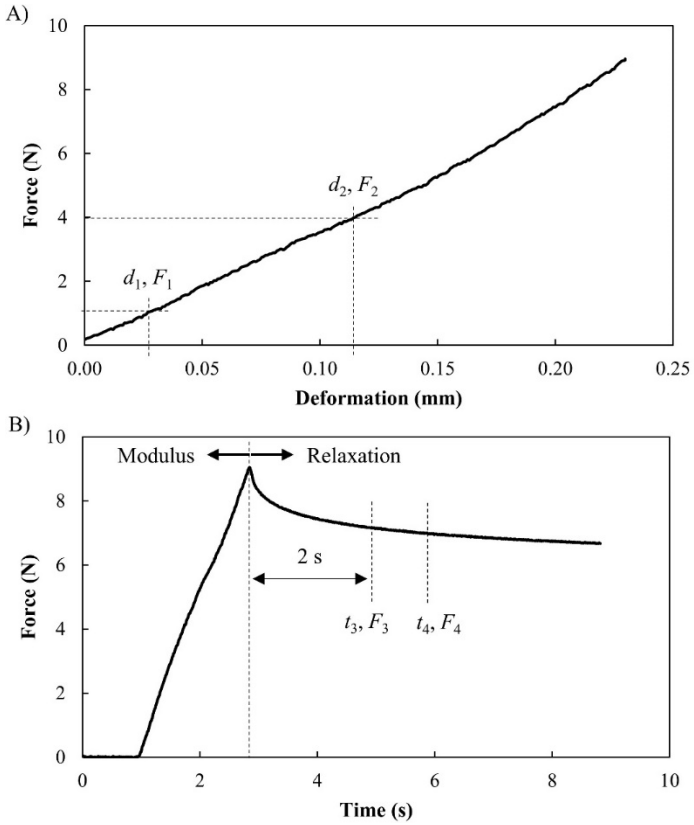

Figure 14. Example plots demonstrating the A) indenter modulus and B) relaxation constant measurement methodology.

5. POLYMER DEGRADATION THEORY

Oxidation is one of the primary degradation mechanisms for polymeric specimens undergoing combined thermal and radiation stress. Hardening at the specimen surface due to oxidation may lead to the initiation of cracks and their propagation through the material cross-section [13]. The generation of free radicals, and their consumption by any antioxidants that may be present within the polymer, affects the rate of oxidation which is also influenced by the aging scenario. For example, previous work has shown that the reaction of free radicals with polymer chains may be the dominant degradation mechanism for the simultaneous aging scenario, whereas free radicals may be predominantly consumed by antioxidants (until depleted) in the sequential aging scenario [38].

5.1 First-Order Reaction Kinetics

First-order reaction kinetics has been routinely used to model the degradation of polymers [39]. As shown in Equation (7), a first-order system may be composed of a rate term (k) dependent upon both temperature (T) and radiation dose (D), and a term correlating the fraction transformed or characteristic value (P) which is dependent on time (t).

$$-\frac{dP}{dt} = k(T, D)P(t) \tag{7}$$

The first-order differential equation shown in Equation (7) is separable and easily solvable, with the solution given by Equation (8), where P_0 is the initial characteristic value.

$$P(t) = P_0 e^{-k(T,D)t} \tag{8}$$

Equations (7) and (8) describe the idealized case where the characteristic value (P) decays exponentially with time. Historically, the rate term (k) is further related to temperature (T) via the Arrhenius equation as shown in Equation (9), where R is the ideal gas constant and A is a pre-exponential factor.

$$k = Ae^{\frac{-E_a}{RT}} \tag{9}$$

An important property for polymeric materials is the overall activation energy (E_a) of degradation. The relationship between the activation energy and the characteristic value (P) is shown in Equation (10).

$$\ln(\ln\frac{P_0}{P(t)}) - \ln t = \ln k = \ln A + \frac{-E_a}{RT} \tag{10}$$

Commonly, the service life of nuclear electrical cables is estimated at a target temperature by extrapolation of the Arrhenius plot ($-\ln t$ vs. $1/T$). However, the functional form of Equation (10) inherently causes large uncertainties when estimating the service life of nuclear electrical cables (potentially on the order of hundreds of years at 40°C). Efforts have been undertaken to reduce the uncertainty of activation energy estimations via low-temperature and long-term aging and ultrasensitive characterization techniques, but investigation into how polymer degradation deviates from first-order reaction kinetics has been limited. Below, two additional analysis methods are implemented to analyze the synergism of aging based on the kinetics of non-first-order reaction kinetics (Section 5.2) and principal component analysis (Section 5.3).

5.2 Deviation from First-Order Reaction Kinetics

In many cases oxidation kinetics deviate from first-order behavior due to the low mobility of polymer chains, the slow transportation of reactive species, the random distribution of free radical scavengers, and the slow removal of oxidation products. Actual oxidation mechanisms are difficult to predict and vary from one chemical structure to another. For simplicity, it is assumed that all effects due to the reduced mobility of polymers within the system can be generalized as a side reaction that generates metastable species. Typical examples of metastable oxidation products are peroxide (ROOR') and hydroperoxide (ROOH), where R and R' represent generic organic groups (hydrocarbons). Breakdown of the metastable species occurs over long time periods and can be accelerated by heat. More specifically, thermal re-initiation will occur when switching from the radiation-aging to thermal-aging scenario. Gillen et al. [40,41] proposed a mechanism to explain the mechanical response of polyethylene (PE) insulation and polyvinyl chloride (PVC) jacket under radiation-to-thermal sequential aging. The simplified elementary steps are shown in Figure 15. In the proposed mechanism, the initiation rate depends on the dose rate (D), whereas the overall reaction rate is not linearly dependent on dose rate. Such nonlinear dose rate dependency explains the dose rate effects observed when there is no diffusion limit [40].

Initiation:

$\text{Polymer} \xrightarrow{k_1 D} \text{R}\cdot$ (D = irradiation dose rate)

Propagation (fast):

$\text{R}\cdot + \text{O}_2 \xrightarrow{k_1'} \text{RO}_2\cdot \quad (k_1 = k_1'[\text{O}_2])$

$\text{RO}_2\cdot + \text{RH} \xrightarrow{k_2'} \text{ROOH} + \text{R}\cdot \quad (k_2 = k_2'\,[\text{RH}])$

$\text{RO}_2\cdot \xrightarrow{k_3} \text{R}\cdot + \text{P}_1$

Propagation (slow):

$\text{ROOH} \xrightarrow{k_4} \text{RO}\cdot + \cdot\text{OH}$ (re-initiation)

$\text{RO}\cdot + \text{RH} \xrightarrow{k_5'} \text{ROH} + \text{R}\cdot \quad (k_5 = k_5'[\text{RH}])$

$\cdot\text{OH} + \text{RH} \xrightarrow{k_6'} \text{H}_2\text{O} + \text{R}\cdot \quad (k_6 = k_6'[\text{RH}])$

Termination:

$\text{RO}_2\cdot \xrightarrow{k_7} \text{P}_2$ (unimolecular termination)

Figure 15. Proposed mechanisms for radiation-to-thermal sequential aging by Gillen et al. [40].

Hydroperoxide (ROOH) in Figure 15 can represent any species that are metastable under low temperatures including trapped free radicals, free radicals temporarily attached to antioxidants, or any caged reactive chemicals due to the low mobility of the polymer chains. ROH and H_2O are representative of volatile chemicals that result from the breakdown of metastable species. Other volatile products such as CO and CO_2 are assumed to follow the same production rate (i.e., proportional to the ROOH consumption rate). It should be noted that unimolecular termination is favored over bimolecular termination since the latter requires two polymeric radicals travelling to the same location, which has a very low probability due to the extremely limited motion of polymer chains.

Mass change of polymeric materials due to degradation depends on the rate of peroxide breakdown (k_4 for slow propagation reactions) and competition between propagation and termination reactions (k_2/k_7). When termination dominates, crosslinking or chain transfer occurs which primarily leads to an increase in

mass. At higher temperatures, the proportion of propagation increases, along with the faster breakdown of metastable species, leading to more volatile small molecules being produced and consequently to a greater decrease in mass. For characterization methods that are indirectly related to the consumption and formation of chemical species, such as elongation at break, it is assumed that the material is degraded when oxidation products P_1 and P_2 accumulate to a certain amount. It is further assumed that the characteristic or product degradation rate is a linear combination of the oxidation products, $[\mathrm{P}] = a[\mathrm{P_1}] + b[\mathrm{P_2}]$. Following a procedure similar to that described in Gillen et al. [40] and starting from a steady-state assumption of $d[\cdot]/dt = 0$, where $[\cdot]$ referring to all types of radicals,

$$\frac{\mathrm{d}[\mathrm{RO}\cdot]}{\mathrm{d}t} = k_4[\mathrm{ROOH}] - k_5[\mathrm{RO}\cdot] = 0$$

$$\frac{\mathrm{d}[\mathrm{OH}\cdot]}{\mathrm{d}t} = k_4[\mathrm{ROOH}] - k_6[\cdot\mathrm{OH}] = 0$$

$$\frac{\mathrm{d}[\mathrm{RO_2}\cdot]}{\mathrm{d}t} = k_1[\mathrm{R}\cdot] - k_2[\mathrm{RO_2}\cdot] - k_3[\mathrm{RO_2}\cdot] - k_7[\mathrm{RO_2}\cdot] = 0$$

$$\frac{\mathrm{d}[\mathrm{R}\cdot]}{\mathrm{d}t} = k_5[\mathrm{RO}\cdot] + k_6[\cdot\mathrm{OH}] + k_3[\mathrm{RO_2}\cdot] + k_2[\mathrm{RO_2}\cdot] - k_1[\mathrm{R}\cdot] + k_1 D = 0$$

The following relationships between the concentration of polymer radicals can be derived,

$$\Longrightarrow 2k_4[\mathrm{ROOH}] + (k_2 + k_3)[\mathrm{RO_2}\cdot] - k_1[\mathrm{R}\cdot] + k_1 D = 0$$

$$\Longrightarrow 2k_4[\mathrm{ROOH}] - k_7[\mathrm{RO_2}\cdot] + k_1 D = 0$$

Since the breakdown of ROOH is the rate-determining step, its consumption rate is given by

$$\frac{\mathrm{d}[\mathrm{ROOH}]}{\mathrm{d}t} = k_2[\mathrm{RO_2}\cdot] - k_4[\mathrm{ROOH}] = \frac{k_2}{k_7}(k_1 D + 2k_4[\mathrm{ROOH}]) - k_4[\mathrm{ROOH}]$$

Solving the ordinary differential equation (ODE) with initial condition $[\mathrm{ROOH}] = 0$ at $t = 0$,

$$[\mathrm{ROOH}] = \frac{k_1 k_2 D}{k_4(2k_2 - k_7)}\left(\exp\frac{k_4(2k_2 - k_7)\cdot t}{k_7} - 1\right)$$

Finally, the degradation product formation rate is given by

$$\frac{d[\mathrm{P}]}{dt} = a\frac{d[\mathrm{P_1}]}{dt} + b\frac{d[\mathrm{P_2}]}{dt} = ak_3[\mathrm{RO_2}\cdot] + bk_7[\mathrm{RO_2}\cdot] = \frac{k_1(ak_3 + bk_7)D + 2(ak_3 + bk_7)k_4[\mathrm{ROOH}]}{k_7}$$

Assuming that the product degradation rate is initially 0 ([P] = 0 at t = 0), [P] as a function of time is found by substituting [ROOH] and solving the ODE,

$$[\mathrm{P}] = \frac{k_1(ak_3 + bk_7)D}{(2k_2 - k_7)}\left\{\frac{2k_2}{k_4(2k_2 - k_7)}\left[\exp\left(\frac{k_4(2k_2 - k_7)}{k_7}t\right) - 1\right] - t\right\}$$

$$= C_1\exp(C_2 t) - C_3 t - C_1 \qquad (11)$$

where

$$C_1 = \frac{k_1 D(ak_3 + bk_7)}{k_7} \frac{1}{k_4} \frac{2k_2/k_7}{(2k_2/k_7 - 1)^2}$$

$$C_2 = k_4(2k_2/k_7 - 1)$$

$$C_3 = \frac{k_1 D(ak_3 + bk_7)}{k_7} \frac{1}{(2k_2/k_7 - 1)}$$

In Equation (11), the linear term $C_3 t$ causes the overall kinetics to deviate from a first-order reaction. Dividing [P] by $k_1 D(ak_3 + bk_7)/k_7$, the remaining terms in Equation (11) depend primarily on k_4 and k_2/k_7.

5.3 Principal Component Analysis

Principal component analysis (PCA) is a statistical approach for summarizing multidimensional data with a smaller number of representative variables. PCA is of growing importance in various research fields where data analysis becomes challenging due to high dimensionality and correlated variables. Here, PCA is applied to data collected for aged nuclear electrical cable insulation by different characterization methods. By analyzing the principal components (PCs) of the collected data, key indicators of insulation degradation can be identified. PCA results can also reveal different degradation pathways caused by the three aging scenarios. Below, the basics methodologies of the PCA approach are discussed [42]. These methodologies are then applied to the characterization results using code written in R (The R Foundation, r-project.org, [43]) following a procedure similar to that developed by Silva et al. [44] in Section 7.2.

For a data set of n observations with measurements on a set of p variables, $X_1, X_2, \ldots, X_p$, PCA computes and seeks a reduced number of dimensions that can correlate most of the variability in the data set. Each of the dimensions calculated by PCA, called a PC, is a normalized linear combination of the p indicators. The first PC direction (Z_1) is selected to maximize the variance of the input data:

$$Z_1 = \phi_{11} X_1 + \phi_{21} X_1 + \cdots + \phi_{p1} X_p$$

The elements $\varphi_{11}, \varphi_{21}, \ldots, \varphi_{p1}$ are the loadings of the first PC (see Figure 9 for an example). The loadings are constrained such that the sum of squares of the loadings is equal to one. With the original observations, the first PC loadings are used to calculate the optimization process shown in Equation (12), where x_{ij} is the value of the jth variable for the ith observation ($i = 1, 2, \ldots, n$ and $j = 1, 2, \ldots, p$) and φ_{j1} is the loading of the jth variable for the first PC:

$$maximize \left\{ \frac{1}{n} \sum_{i=1}^{n} \left(\sum_{j=1}^{p} \phi_{j1} x_{ij} \right)^2 \right\} \tag{12}$$

which is subjected to the following constraint

$$\sum_j^p \phi_{j1}^2 = 1$$

After PCA optimization, the projected values on the first PC direction are given by Equation (13), where $z_{11}, z_{21}, \ldots, z_{n1}$ are defined as the scores of the first PC.

$$z_{i1} = \phi_{11} x_{i1} + \phi_{21} x_{i2} + \cdots + \phi_{p1} x_{ip} \tag{13}$$

The outputs of PCA include the eigenvalues and eigenvectors of the covariance matrix calculated from the normalized data. The eigenvectors of each PC define the directions of the new feature space along which most data variation occurs. PCA serves as an attractive tool for data visualization through the usage of informative data plots, such as a score plot whereby grouping of samples or patterns in the data set can be observed and the loading plot which is useful to identify which variables are responsible for the grouping or patterns observed in the score plot.

6. RESULTS OF SIMULTANEOUS VERSUS SEQUENTIAL AGING CHARACTERIZATION

The characterization results for the simultaneous (*T/R*) and sequentially (*T+R*, *R+T*) aged insulation specimens are discussed below. For all figures, the error ranges were calculated as the standard deviation of the specimen measurements. In addition, curve fitting to the respective equations in Section 5 was conducted using the MATLAB® curve fitting application with a nonlinear least squares approach (trust region algorithm) to minimize the sum of squares of the residuals.

6.1 Mass Change

The measured mass change (Δm) of the insulation specimens after aging is compared to that of the unaged insulation specimens as shown in Figure 16; details regarding the Δm trends and the evaluated model parameters are summarized in Table 5 and Table 6, respectively. At 3 days of exposure (20 kGy), the *T+R*, *R+T*, and *T* (temperature only) aging scenarios produced an increase in specimen mass of approximately 2.5% for XLPE and 1.5% for EPDM. For both material types, the *T/R* and *R* (radiation only at 26°C) aging scenarios produced minor variations in mass at exposures less than 25 days (< 250 kGy); a small positive linear slope (between $1.1\text{x}10^{-2}$ to $4.0\text{x}10^{-3}$ percent per day of exposure) was measured for the *T/R* and *R* aging scenarios after the initial exposure (3 days, 20 kGy). However, at a higher exposure (36 days, 260 kGy) the *T/R* aging scenario produced a rapid, linear decrease in the measured mass for the EPDM specimens (an approximate drop of 3% from a dose of 260 kGy to 320 kGy), which correlates to a decrease in EAB measurements to be discussed next. A negative linear trend (between $-1.6\text{x}10^{-2}$ to $-5.3\text{x}10^{-2}$ percent per day of exposure) was observed for Δm in the *T+R*, *R+T*, and *T* aging scenarios after initial exposure (3 days, 20 kGy) for both material types, opposite to that found for the *T/R* and *R* aging scenarios. Similar to the *T/R* aging scenario, the *R+T* aging scenario for EPDM produced a rapid linear decrease (an approximate decrease of 9% from 170 kGy to 320 kGy) in the measured mass after 23 days of exposure (170 kGy).

Table 5. The linear slope in Δm after initial exposure (3 days); a second linear slope was observed for EPDM with the *T/R* and *R+T* aging scenarios after 23 days and 36 days of exposure, respectively.

Type	Aging Scenario	Initial (%)	Slope 1 (%/day)	Slope 2 (%/day)
XLPE (RSCC)	*T/R*	0.10	$3.86\text{x}10^{-3}$	--
	T+R	2.74	$-1.57\text{x}10^{-2}$	--
	R+T	2.41	$-2.84\text{x}10^{-2}$	--
	T	2.72	$-3.44\text{x}10^{-2}$	--
	R	0.08	$1.08\text{x}10^{-2}$	--
EPDM (Dekoron®)	*T/R*	-0.56	$8.27\text{x}10^{-3}$	$-3.48\text{x}10^{-1}$
	T+R	1.68	$-1.88\text{x}10^{-2}$	--
	R+T	1.06	$-5.26\text{x}10^{-2}$	$-4.17\text{x}10^{-1}$
	T	1.68	$-4.89\text{x}10^{-2}$	--
	R	-0.35	$7.14\text{x}10^{-3}$	--

EPDM = ethylene-propylene-diene elastomer; XLPE = cross-linked polyethylene.

Table 6. Evaluated model parameters for Δm using Equation (11). Fitting was conducted for two insulation specimens using MATLAB® curve fitting software to minimize the sum of squares of the residuals.

Type	Aging Scenario	k_2/k_7	k_4	$1/(k_1*D)$
XLPE (RSCC)	*T/R*	--	--	--
	T+R	0.498	200	53.0
	R+T	0.498	400	30.0
	T	0.498	400	27.0
	R	0.000	--	86.0
EPDM (Dekoron®)	*T/R*	0.750	0.180	350
	T+R	0.495	75.0	40.0
	R+T	0.200	0.0500	0.300
	T	0.495	150	20.0
	R	0.000	--	246

EPDM = ethylene-propylene-diene elastomer; XLPE = cross-linked polyethylene.

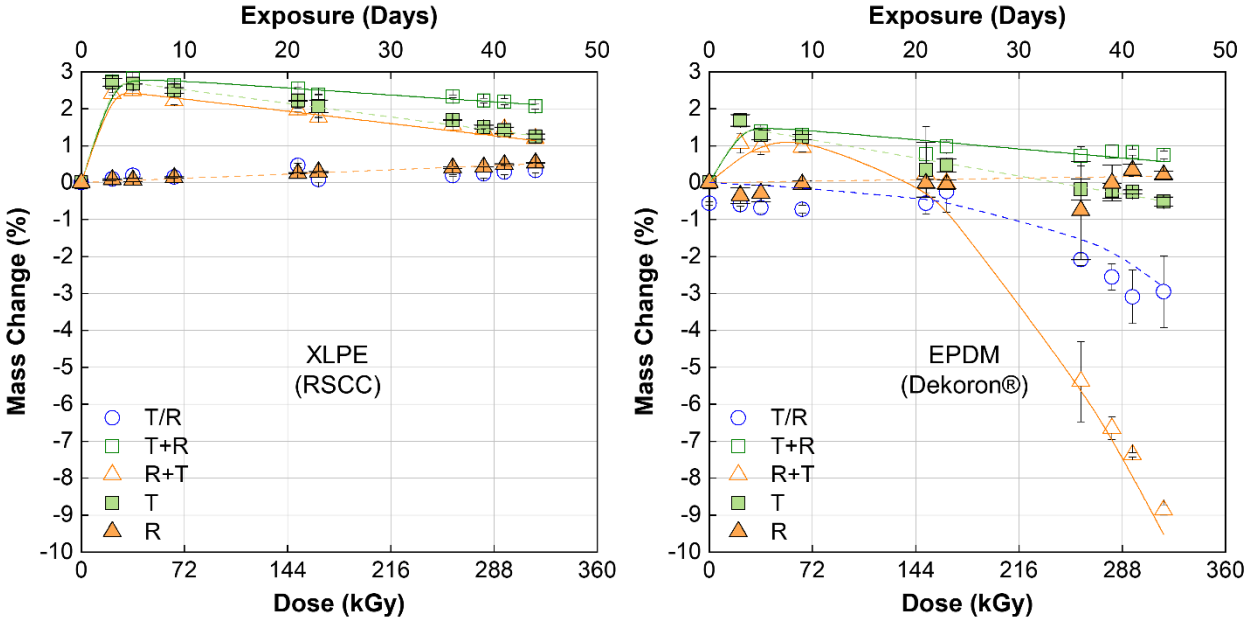

Figure 16. The average Δm of the (left) XLPE and (right) EPDM insulation specimens after aging. *T* represents thermal aging only (150°C) and *R* represents radiation aging at room temperature (26°C, 300 Gy/hr). The solid and dashed lines represent fitting of the data for two insulation specimens to the model in Equation (11) using the parameters of Table 6.

The mass changes for each exposure step in the sequential aging scenarios are shown in Figure 17 for the effect of radiation after thermal aging and in Figure 18 for the effect of heating after irradiation. For both material types, a similar effect was observed with the application of radiation after thermal aging: the measured insulation mass increased by approximately 0.024% per day of exposure (or approximately 3.4×10^{-3} percent per absorbed kGy). Interestingly, this increase in mass is greater than that observed for irradiation alone (for example, a mass change of 0.011% and 0.0071% per day of exposure was measured for the *R* only aging scenario for XLPE and EPDM, respectively). On the other hand, differences were

observed between the material types for heating applied after irradiation, as illustrated by the sharp decrease in mass change for the EPDM specimens. For XLPE, with the application of thermal aging after irradiation, an initial increase in mass at lower exposure (3 days, 20 kGy) was followed by a linear decrease in mass (-0.04% per day exposure). A similar linear decrease in mass was measured for EPDM up to 23 days exposure (-0.06% per day exposure), but a sharp linear decrease was measured after this exposure (-0.43% per day exposure after 23 days), which correlates to a sharp decrease in EAB.

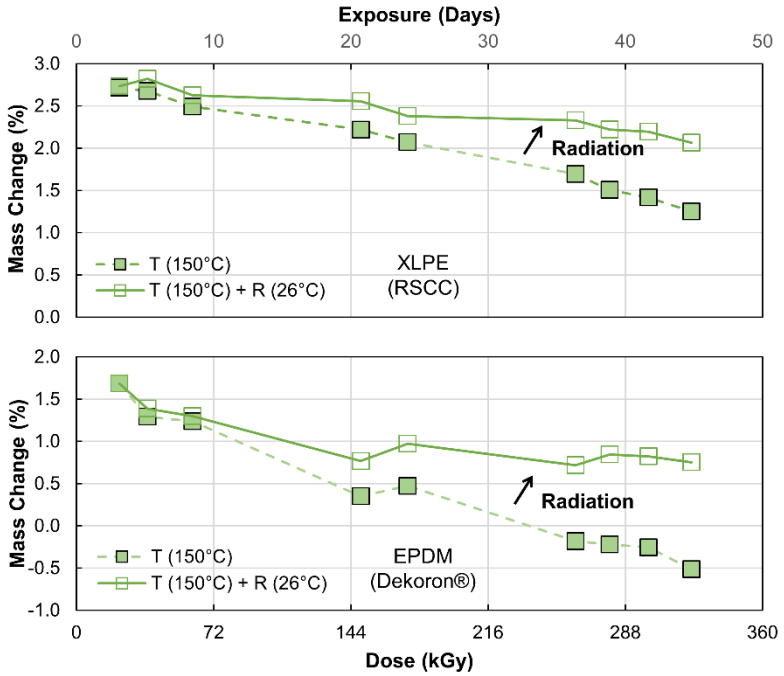

Figure 17. The average Δ*m* due to irradiation (300 Gy/hr) after thermal aging (150°C) for (top) XLPE and (bottom) EPDM.

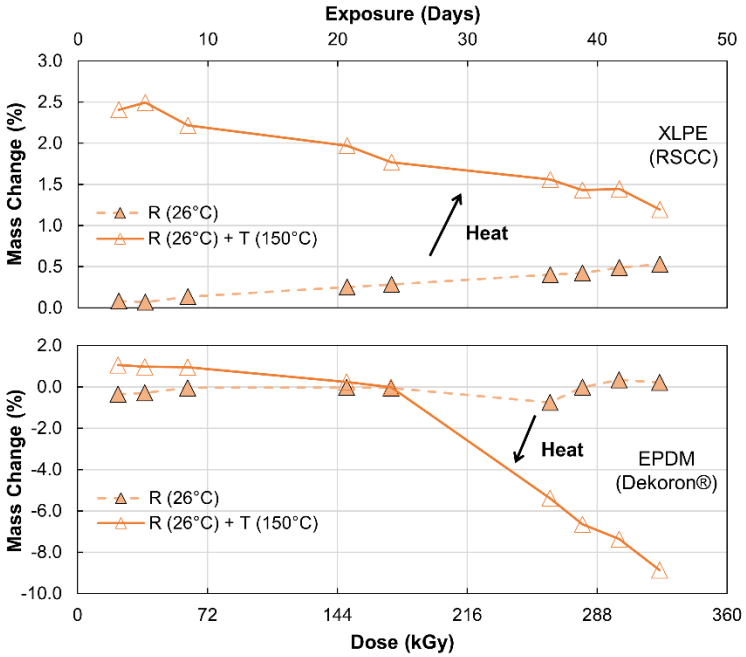

Figure 18. The average Δm due to heating (150°C) after irradiation (300 Gy/hr) for (top) XLPE and (bottom) EPDM.

6.2 Elongation at Break

The measured, averaged and normalized (with respect to the unaged specimens) EAB of the aged insulation specimens using video extensometry is shown in Figure 19. Parameters curve fit to Equation (11) are shown in Table 7. A roughly sigmoidal, or S-shaped, curve [45] was observed for both material types and all three aging scenarios. The unaged XLPE specimens were likely not fully cured prior to aging as these specimens produced a reduced EAB (approximately 224%) when compared to the specimens at low exposure (3 days, 20 kGy, approximately 272% EAB). In this report, specimen end-of-life, or when the specimens were considered operationally degraded, was defined conservatively as 50% of the unaged EAB and to occur at the critical time, t_c [3]. Here, it was observed that the critical time depends both upon the aging scenario and the material type. A critical time of 38 days (276 kGy) for the *T/R* aging scenario, 28 days (203 kGy) for the *T*+*R* aging scenario, and 44 days (320 kGy) for the *R*+*T* aging scenario was estimated for XLPE. Thus, for XLPE, the critical time of the *T*+*R* sequential aging scenario was estimated to be approximately 74% of the *T/R* simultaneous aging scenario. Because the simultaneous aging scenario may be more likely to occur in service, this result may indicate that laboratory sequential aging (thermal aging and then gamma irradiation [3]) may be conservative for XLPE in the prediction of cable lifetime. Also, the critical time of the *R*+*T* aging scenario was measured to be approximately 116% of that for the simultaneous aging scenario, possibly indicating that this aging sequence is less conservative for XLPE than what may occur under actual service conditions. In contrast, an opposite trend was measured for EPDM. Measured critical times of 28 days (203 kGy) for the *T/R* aging scenario, 31 days (225 kGy) for the *T*+*R* aging scenario, and 18 days (130 kGy) for the *R*+*T* aging scenario were estimated for EPDM. With EPDM, the lowest critical time was measured for the *R*+*T* aging scenario and was approximately 64% of that measured for the *T/R* simultaneous aging scenario. The laboratory aging scenario, *T*+*R*, produced an estimated critical time that was greater than the *T/R* aging scenario (111%).

Table 7. Evaluated model parameters for EAB using Equation (11) and the estimated critical time, t_c. Fitting was conducted using MATLAB® curve fitting software to minimize the sum of squares of the residuals.

Type	Aging Scenario	k_2/k_7	k_4	$1/(k_1*D)$	t_c (day)
XLPE (RSCC)	*T/R*	0.510	0.725	1000	38
	T+R	0.510	1.23	1000	28
	R+T	0.510	0.550	1000	44
EPDM (Dekoron®)	*T/R*	0.510	3.00	5000	28
	T+R	0.510	0.0370	100	31
	R+T	0.510	0.060	55.0	18

EPDM = ethylene-propylene-diene elastomer; XLPE = cross-linked polyethylene.

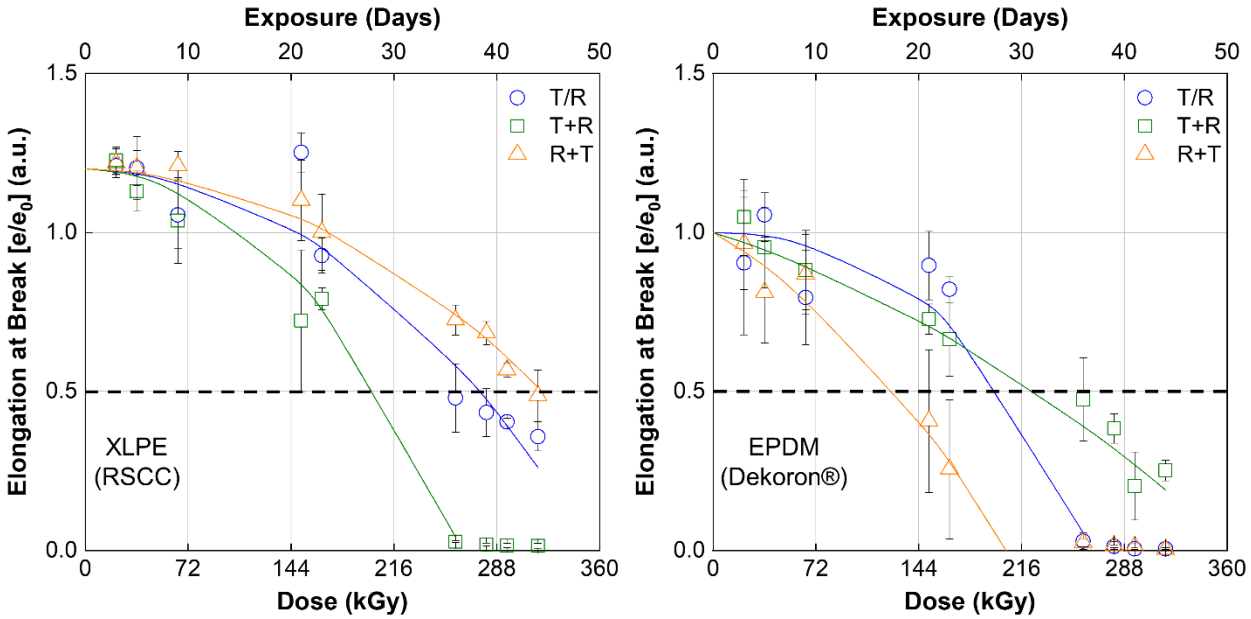

Figure 19. The averaged and normalized EAB analyzed using video extensometry for the aged (left) XLPE and (right) EPDM insulation specimens. The solid lines represent fitting of the data to the model in Equation (11) using the parameters of Table 7.

6.3 Carbonyl Index

The measured FTIR ATR spectra for samples at selected absorbed doses are shown in Figures 20 and 21 for XLPE and EPDM, respectively. For increasing exposure (absorbed dose), stronger carbonyl absorption peaks (C=O, 1715 cm^{-1}) were measured for both material types and all aging scenarios, with the largest absorption occurring at the highest exposure (44 days, 320 kGy). Conversely, a decrease in the methylene absorption peak (C-H, 2848 cm^{-1}) was found for increasing exposure, with the smallest absorption occurring at the highest exposure. The relative change in the peak absorption for these functional groups was previously defined as the CI (vide supra) and is shown in Figure 22. The CI is a convenient metric for oxidation because the carbonyl groups are common oxidation byproducts and methylene groups form a common backbone for both XLPE and EPDM. Curve fitting parameters of the CI to the model of Equation (11) are shown in Table 8. For both material types and all aging scenarios, the CI increased with

increasing exposure. A re-initiation rate constant, k_4, with value less than 1 was estimated for the XLPE specimens, possibly indicating that oxidation is limited with this material type (similar to that observed for the *T*+*R* aging scenario for EPDM). A surprising result was observed for the XLPE specimens undergoing the *T*+*R* aging scenario. For XLPE and at the highest exposure of 44 days (320 kGy), the largest CI was measured for the *T/R* aging scenario (0.44), while the lowest CI was measured for the *T*+*R* aging scenario (0.26). However, for XLPE at this exposure, the specimens undergoing the *T*+*R* aging scenario appeared to be much more degraded (i.e., brittle) than the specimens undergoing the *T/R* aging scenario (3% EAB for the *T*+*R* specimens vs. 80% EAB for the *T/R* specimens); therefore, for the exposure conditions and dose rate explored here, this result may support the hypothesis that oxidation is not the primary degradation mechanism for XLPE. Conversely, the re-initiation rate constant was estimated to be greater than 1 for the EPDM specimens (*T/R* and *R*+*T* aging scenarios). Measurements of the CI for EPDM at high exposures were more in line with expectations as the specimens with the highest CI (1.7 for *T/R* at 320 kGy and 1.3 for *R*+*T* at 300 kGy) correspondingly had the lowest EAB (2% EAB for *T/R* at 320 kGy and 1% EAB for *R*+*T* at 320 kGy), while the specimen with the lowest CI (*T*+*R*, 0.4 at 320 kGy) had the highest EAB (96% EAB at 320 kGy).

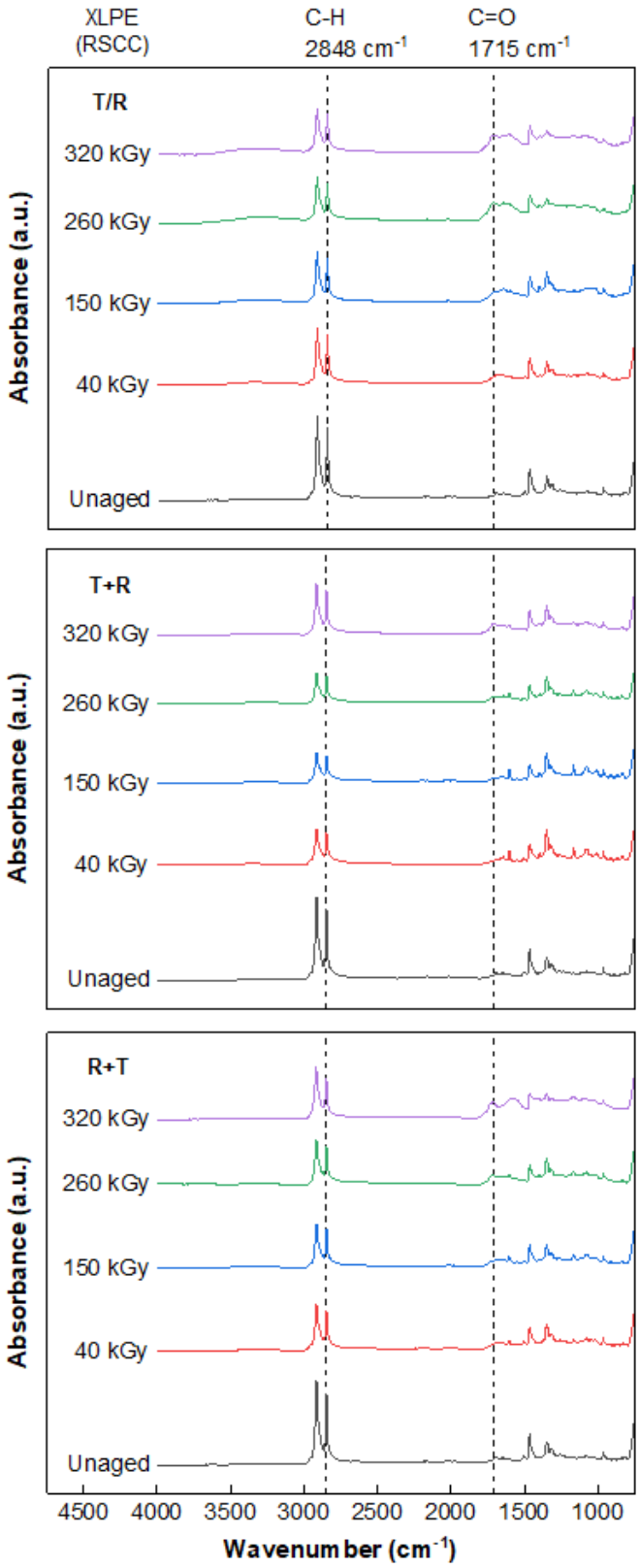

Figure 20. FTIR absorbance spectra for the XLPE insulation specimens. The carbonyl (1715 cm^{-1}) and methylene (2848 cm^{-1}) peaks are indicated.

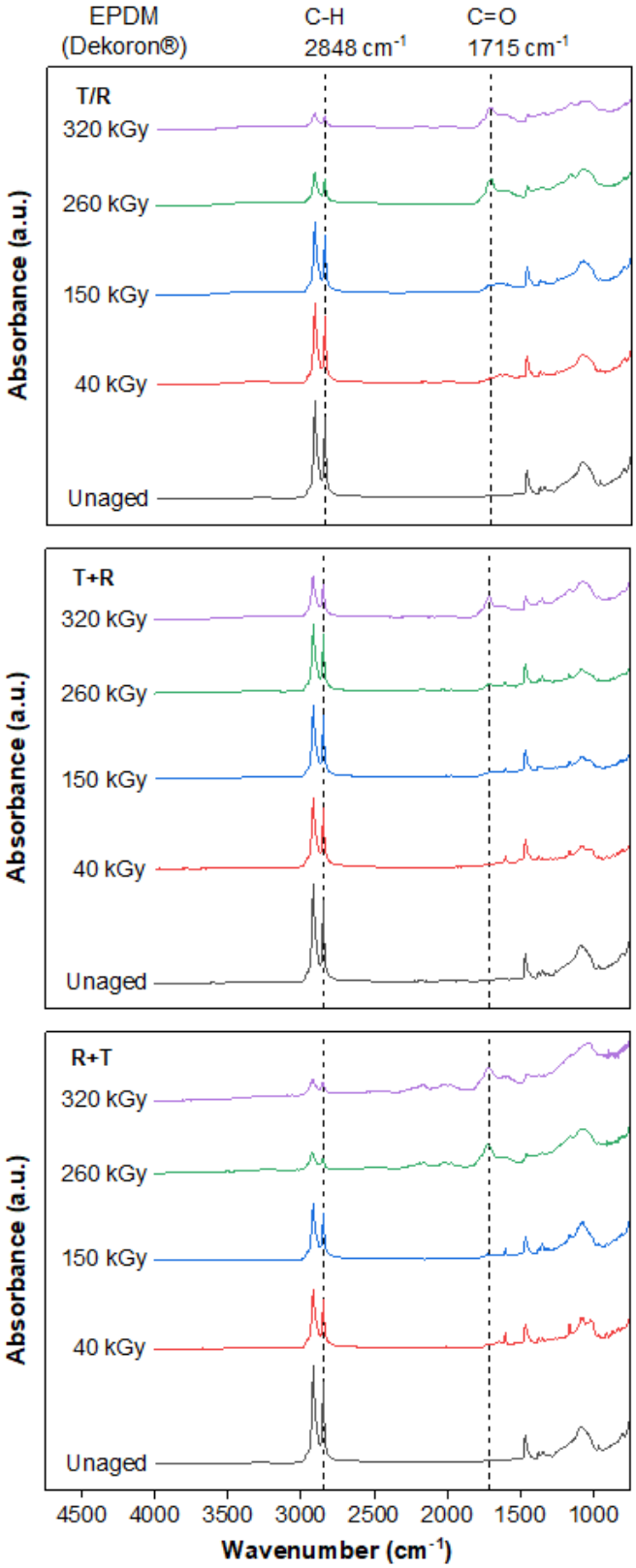

Figure 21. FTIR absorbance spectra for the EPDM insulation specimens. The carbonyl (1715 cm^{-1}) and methylene (2848 cm^{-1}) peaks are indicated.

Table 8. Evaluated model parameters for CI using Equation (11). Fitting was conducted using MATLAB® curve fitting software to minimize the sum of squares of the residuals.

Type	Aging Scenario	k_2/k_7	k_4	$1/(k_1*D)$
XLPE (RSCC)	*T/R*	0.510	0.450	1000
	T+R	0.510	0.158	1000
	R+T	0.510	0.147	1000
EPDM (Dekoron®)	*T/R*	0.510	1.56	1500
	T+R	0.510	0.400	1500
	R+T	0.510	1.40	1500

EPDM = ethylene-propylene-diene elastomer; XLPE = cross-linked polyethylene.

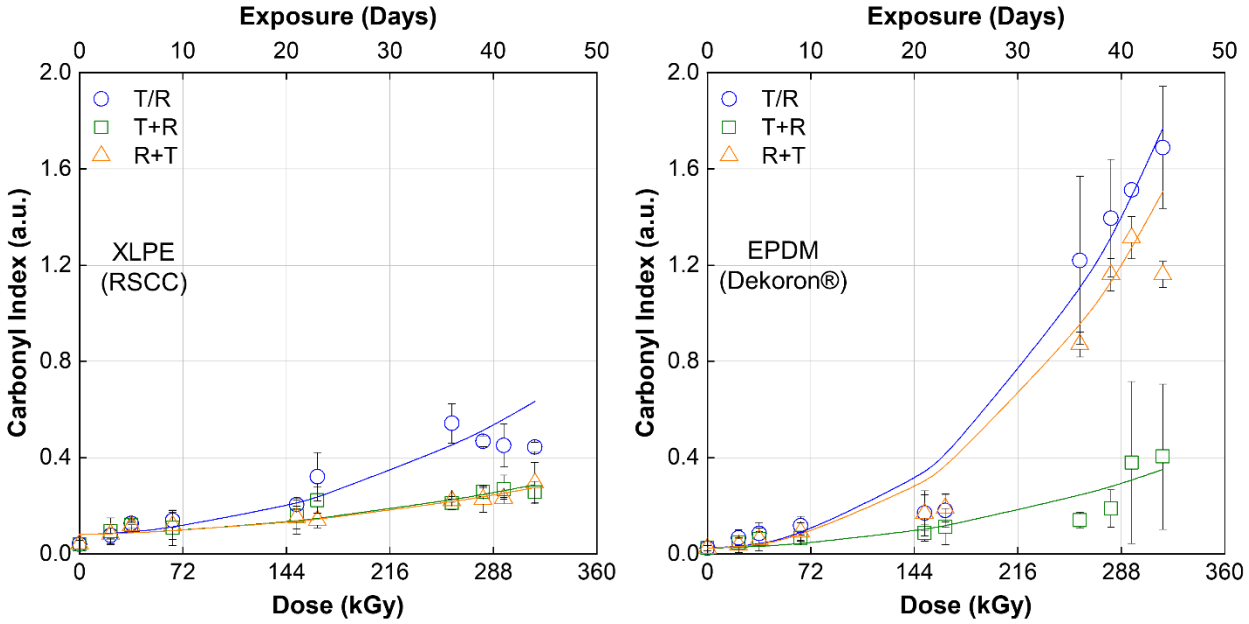

Figure 22. The average CI of the (left) XLPE and (right) EPDM insulation specimens after aging. The solid lines represent fitting of the data to the model in Equation (11) using the parameters of Table 8.

6.4 Total Color Difference

Digital images of the aged insulation specimens at select exposures are shown in Figure 23. For both material types, increasing coloration of the insulation specimens was observed with increasing exposure; the XLPE specimens tended toward yellow and the EPDM specimens became darker (reddish). Therefore, it is likely that quantifying color change would have been more difficult using the Yellowness Index for the EPDM specimens. The total color difference approach incorporated here accounts for variations in specimen darkness, making this approach applicable for the current material types. The average total color difference for the insulation specimens is shown in Figure 24 for both material types. It should be noted that, due to the specimens being tubular in shape, reflection and shadowing on specimen surfaces produced scattering of the measured color data. Similar to that qualitatively apparent to the observer, the total color difference increased with increasing exposure, as observed in previous work [46]. For XLPE, all aging scenarios appeared to converge, or plateau (referred to herein as the equilibrium color difference), at high

exposures; for example, after 23 days of exposure (170 kGy) only small variations were measured in the total color difference for XLPE. However, differences were observed in the magnitude of the equilibrium color difference; the largest equilibrium color difference (23 for the *T+R* aging scenario) corresponded to the aging scenario that had the lowest EAB (3% EAB for the *T+R* aging scenario at 44 days exposure). Interestingly, the total color difference increased rapidly for the *R+T* aging scenario (XLPE), compared to the *T/R* or *T+R* aging scenarios, at low exposure; for example, at 3 days of exposure and 20 kGy dose, a ΔE^*_{ab} of 8.8, 9.5, and 15 was measured for the *T/R*, *T+R*, and *R+T* aging scenarios, respectively. Conversely, for EPDM, while the *T+R* aging scenario plateaued at approximately 23 days of exposure, both the *T/R* and *R+T* aging scenarios had yet to plateau for the exposures investigated. Even so, an equilibrium color difference was estimated based upon the trend of the data: 38 for the *R+T* aging scenario and 35 for the *T/R* aging scenario, again in line with expectations from EAB measurements. Similar to those observed for XLPE, the EPDM specimens demonstrated large color variations at low exposure for the *R+T* aging scenario: 13, 13, and 19 for the *T/R*, *T+R*, and *R+T* aging scenarios, respectively.

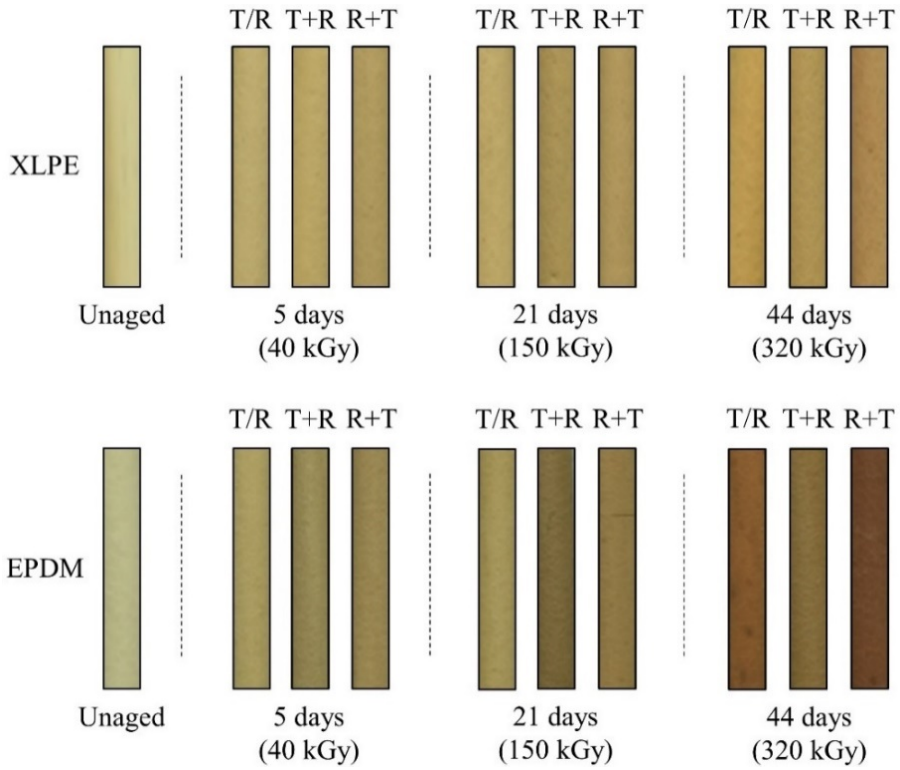

Figure 23. Original color digital images of the (top) XLPE and (bottom) EPDM specimens for select exposures.

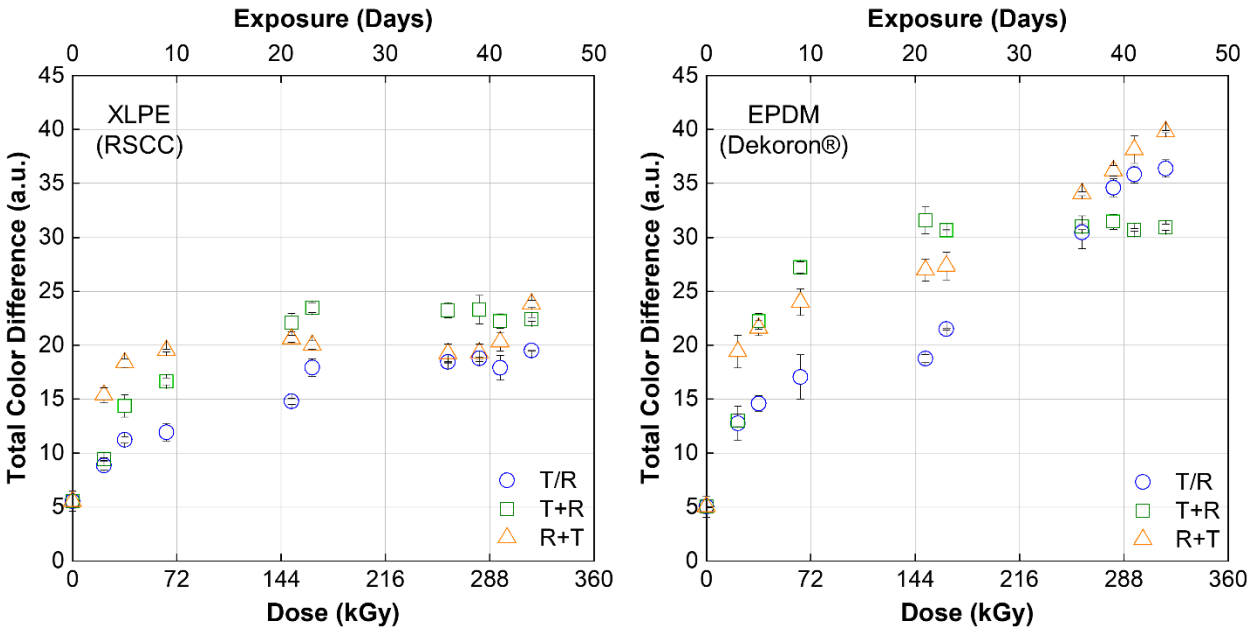

Figure 24. The average total color difference of the (left) XLPE and (right) EPDM insulation specimens after aging.

6.5 Indenter Modulus and Relaxation Constant

The measured IM and τ values of the insulation specimens after aging are shown in Figure 25 and Figure 26, respectively. The evaluated model parameters are summarized in Table 9 and Table 10 for the IM and τ, respectively. For XLPE, the IM, which is an indicator of the compressive stiffness of the material, was found to be insensitive to the *T+R* aging scenario. On the other hand, the *R+T* and *T/R* aging scenarios demonstrated a decrease in the IM of approximately 19% at the highest exposure of 320 kGy. The τ, which is an indicator of the recovery behavior of a deformed material, was found to be more sensitive to aging for XLPE. All aging scenarios demonstrated similar τ values up to an exposure of 144 kGy. Afterwards, the *R+T* and *T/R* aging scenarios exhibited an exponential-like growth in τ leading to an approximate 44% increase in τ at the highest exposure of 320 kGy. Conversely, the *T+R* aging scenario produced a modest increase in τ at the highest exposure (8% increase at 320 kGy). In case of EPDM, the IM and τ trended differently when compared to XLPE. All three aging scenarios demonstrated an increase in IM as a function of exposure. The increase in IM at the highest exposure when compared to the unaged specimens was found to be the greatest in *R+T* aging scenario (195% increase), followed by the *T/R* aging scenario (82% increase), and then the *T+R* aging scenario (50% increase). On the other hand, τ values of aged EPDM insulation specimens did not exhibit any meaningful relationship as a function of exposure, unlike the increasing trends observed for XLPE.

IM and τ, although obtained from the same indentation measurement technique, probe different material properties. The IM measures the elastic property of a viscoelastic polymer, whereas τ measures the viscous behavior of viscoelastic materials [47]. In the case of XLPE, the elastic behavior was less susceptible to aging when compared to the viscous behavior. Conversely, in the case of EPDM, the elastic behavior for radiation first (*R+T*) sequential aging was more susceptible to aging than the viscous response, which demonstrated inconclusive behavior.

Table 9. Evaluated model parameters for IM using Equation (11). Fitting was conducted using MATLAB® curve fitting software to minimize the sum of squares of the residuals.

Type	Aging Scenario	k_2/k_7	k_4	$1/(k_1*D)$
XLPE (RSCC)	*T/R*	0.510	0.0250	-7.40[1]
	T+R	0.510	3.00	5000
	R+T	0.510	0.0100	-6.40[1]
EPDM (Dekoron®)	*T/R*	0.510	2.90	500
	T+R	0.510	0.060	11.0
	R+T	0.510	4.30	500

EPDM = ethylene-propylene-diene elastomer; XLPE = cross-linked polyethylene. [1]Negative value indicates inverse correlation between [P] and IM.

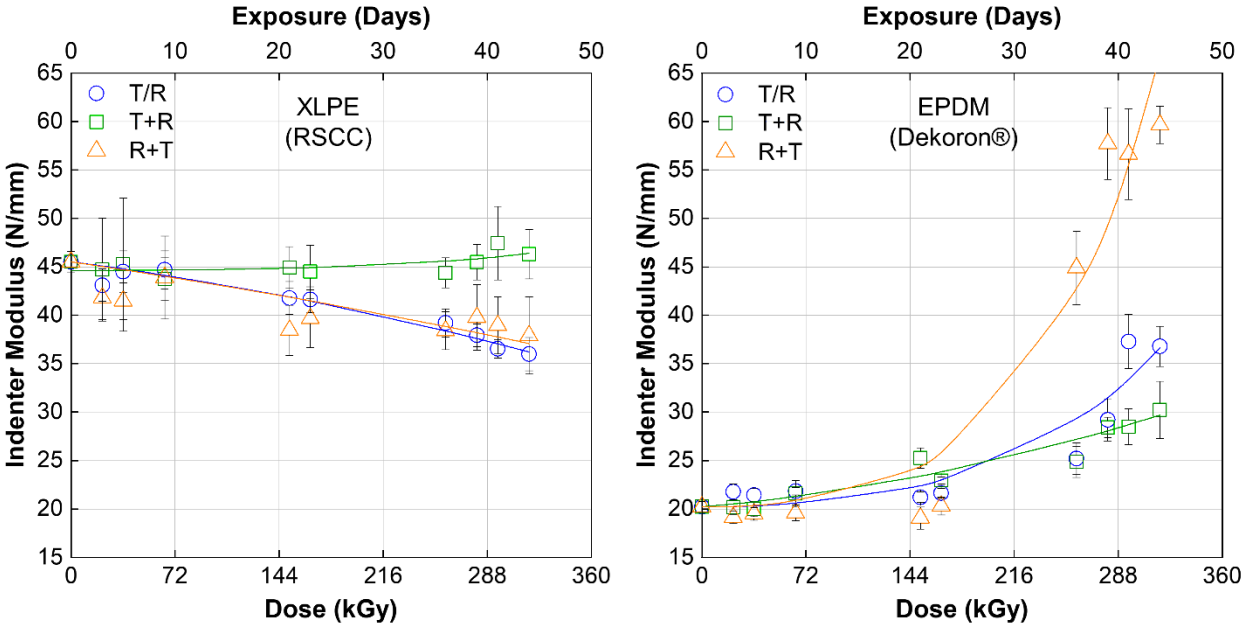

Figure 25. The average IM of the (left) XLPE and (right) EPDM insulation specimens after aging. The solid lines represent fitting of the data to the model in Equation (11) using the parameters of Table 9.

Table 10. Evaluated model parameters for τ using Equation (11). Fitting was conducted using MATLAB® curve fitting software to minimize the sum of squares of the residuals.

Type	Aging Scenario	k_2/k_7	k_4	$1/(k_1*D)$
XLPE (RSCC)	*T/R*	0.510	3.35	500
	T+R	0.510	0.010	11.0
	R+T	0.510	3.15	500
EPDM (Dekoron®)	*T/R*	--	--	--
	T+R	--	--	--
	R+T	--	--	--

EPDM = ethylene-propylene-diene elastomer; XLPE = cross-linked polyethylene.

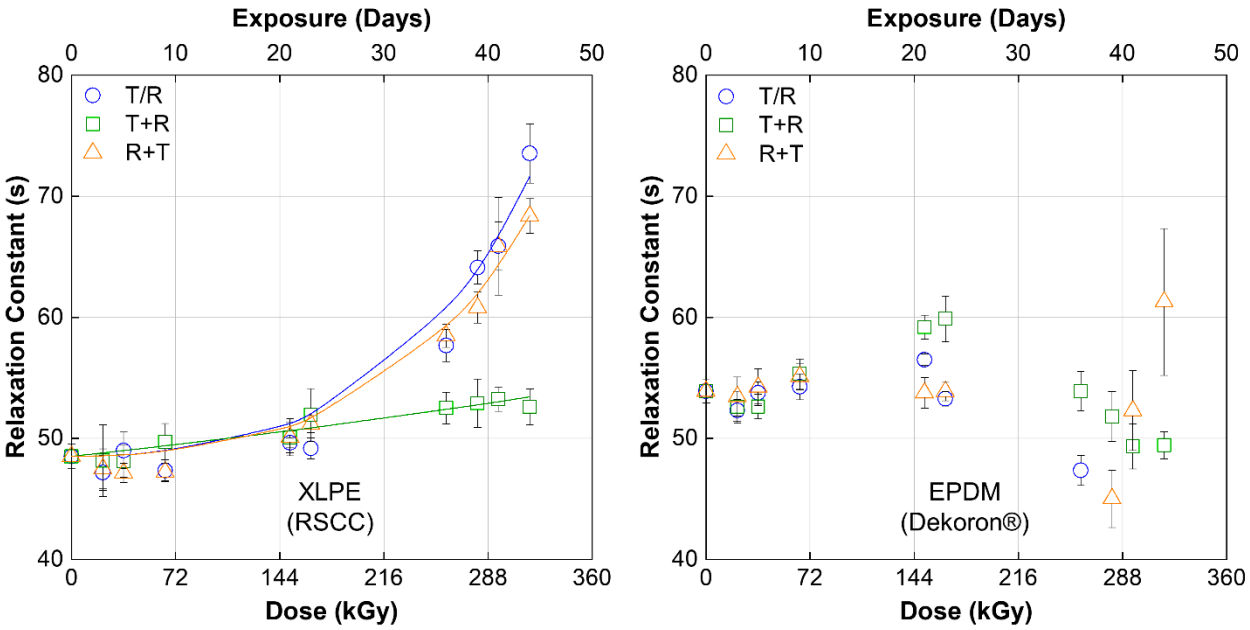

Figure 26. The average τ of the (left) XLPE and (right) EPDM insulation specimens after aging. The solid lines represent fitting of the data to the model in Equation (11) using the parameters of Table 10.

7. DISCUSSION OF CHARACTERIZATION RESULTS

7.1 Mechanisms of Polymer Degradation

The generation of free radicals through thermal exposure, radiation, mechanical forces, and/or catalysis [48] is a primary pathway for the degradation of polyolefin polymers by means of oxidative reactions. The process of free radical generation is partially self-sustaining in the presence of oxygen as additional free radicals are formed, some unstable [49] and others stable forming ketones (e.g. carbonyl groups). The reaction rate will increase with increasing temperature and additional free radicals will be generated with increased irradiation due to an enhanced probability of chain scission. The propagation of this degradation process is much faster than the initiation [48], and this is especially true in the presence of antioxidants. For this reason, an induction time is commonly observed in Δm and for EAB and CI. In addition, the degradation rate of polymers at higher temperatures also plays an important role [50] because loss of integrity can lead to early failure. As observed in Section 6.1, Δm of XLPE and EPDM with radiation-only (*R*) exposure linearly increased as peroxide and hydroperoxide species were generated during irradiation, as shown in Figure 15. Furthermore, as the Δm of the radiation-only conditions is directly proportional to the initiation rate constant (k_1) as shown below, a reduced Δm or slope (see Table 5) was observed when compared to the other aging scenarios due to the lower degradation temperature (26°C vs. 150°C). A similar response was found for the *T*+*R* aging scenario during the second aging step; the application of radiation after thermal aging produced a linear increase of mass with increasing exposure for both material types, see Figure 17.

$$\Delta m \propto -[\mathrm{O}_2] = k_1[\mathrm{R}\cdot]t$$

On the other hand, the abrupt increase in mass for the *R*+*T* aging scenario for both XLPE and EPDM is hypothesized to be primarily due to an accelerated accumulation of metastable species as the temperature during the second aging step is increased. However, this process is short-lived as the breakdown of thermally weak species, such as [ROOH], generate volatile species (e.g., ROH, H_2O, CO_2, CO, CH_4, etc.) which lead to loss of mass with increasing exposure. This mechanism is also potentially responsible for the mass change trends observed for the thermal aging step of the *T*+*R* aging scenario. Thus, for sequential aging, the effects of thermal and radiation aging appear to be independent, although it is assumed there is an induction period for Δm for the *R*+*T* aging scenario as demonstrated by the large mass loss for EPDM above 23 days exposure. For the simultaneous aging scenario (*T*/*R*), it is hypothesized that competition between side reactions and the overall termination reaction produces a relatively minor mass change during the induction period, after which mass decreases rapidly.

Densification of polymeric materials is an indication of degradation and it is assumed that densification is linearly correlated with product degradation rate by $\rho = \rho_0 + k[\mathrm{P}]$, where ρ_0 is the initial density. Density variation of the aged insulation specimens is shown in Figure 27 for XLPE and EPDM. For XLPE, only a mild increase in the density was measured with increasing exposure for all aging scenarios indicating the density of this material type is relatively stable at the exposures and dose rate explored here. Conversely, an increase in density of approximately 20% was observed for the *T*/*R* and *R*+*T* aging scenarios at an exposure of 320 kGy for EPDM, whereas an increase of only 4% was measured for the *T*+*R* aging scenario under the same condition. These results for EPDM are consistent with the material response observed for EAB (Figure 19), CI (Figure 22), and the IM (Figure 25) further indicating that the *T*+*R* aging scenario is the least severe aging scenario for this material type. This occasion of reduced degradation with the *T*+*R* aging scenario (EDPM) might be attributed to the repairing of degraded regions during the irradiation step. It is further hypothesized that the increased degradation of the *T*/*R* and *R*+*T* aging scenarios for EPDM is due to an increased propensity for side reactions and faster breakdown of peroxides as given by the increased rate constant (k_4) in Table 11.

Table 11. Evaluated model parameters for density using Equation (11). Fitting was conducted using MATLAB® curve fitting software to minimize the sum of squares of the residuals.

Type	Aging Scenario	k_2/k_7	k_4	$1/(k_1*D)$
XLPE (RSCC)	*T/R*	0.300	0.660	10000
	T+R	0.300	0.660	3200
	R+T	0.300	0.660	2000
EPDM (Dekoron®)	*T/R*	0.510	0.170	800
	T+R	0.510	0.0100	800
	R+T	0.510	0.160	800

EPDM = ethylene-propylene-diene elastomer; XLPE = cross-linked polyethylene.

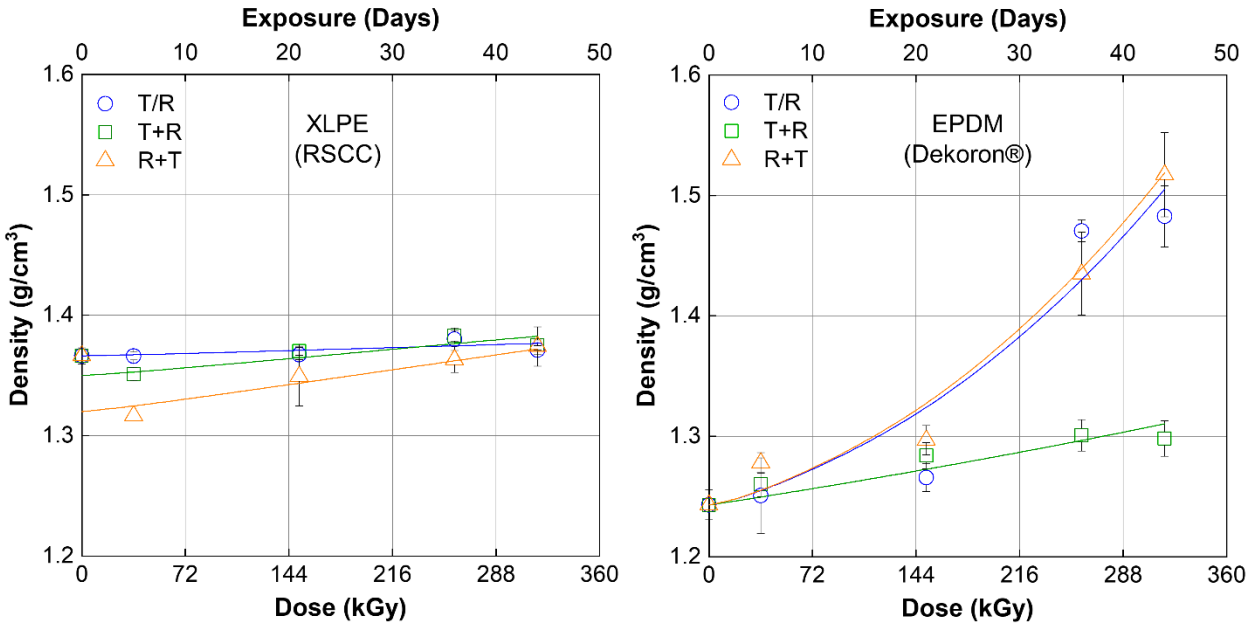

Figure 27. The average density of the (left) XLPE and (right) EPDM insulation specimens after aging. The solid lines represent fitting of the data to the model in Equation (11) using the parameters of Table 11.

As with density, the product degradation rate is assumed to be linearly correlated to EAB (e/e_0 = 1 - [P]) and CI ($CI = CI_0$ + [P]), where the subscript 0 indicates the respective value of the unaged specimen. For EAB, the increased degradation due to the *T+R* aging scenario for XLPE is potentially attributed to further cross-linking during the radiation step, leading to increased brittleness of the specimens and failure at earlier exposures when compared to the *T/R* and *R+T* aging scenarios. The second step (thermal) during the *R+T* aging scenario may primarily be localized and therefore have produced a reduced effect on mechanical properties. An opposite effect was found for EAB measurement of EPDM; reduced degradation was observed for the *T+R* aging scenario, which correlates to the condition with the slowest rate of [ROOH] breakdown (k_4). This trend was also observed for both CI and IM for EPDM. For CI, correlation to any specific mechanism is difficult as the product degradation rate ([P]) does not differentiate between different oxidation products (oxidation products with and without carbonyl groups are all included in [P]); therefore, an improved kinetics model to account for different oxidation products would be useful for future investigations.

7.2 Principal Component Analysis of the Aging Scenarios

As discussed in Section 5.3, PCA allows for distinguishing key indicators of cable insulation degradation by reducing the dimensionality of the data. The accumulated data for both XLPE and EPDM in all three aging scenarios was tabulated for Δm, EAB, CI, total color difference, IM, and τ. The tabulated data was then standardized to have a mean centered at 0 and a variance of 1. Following the work of Silva et al. [44], PCA was applied to the standardized data. Here, the first two PCs, which account for 80% and 87% of the variability in the data for XLPE and EPDM, respectively, were selected for discussion. Two PCA plots are included below: the variable correlation plot (Figure 28) and the score plot (Figure 29). The variable correlation plot correlates the variations in the data between the different characterization methods; a unit circle is also included in the plot – the closer the PCA vectors are to the unit circle, the better the first and second PCs (PC1 and PC2) represent the variability in the data. PCA vectors that are pointing in opposite directions indicate that the data is inversely correlated (e.g., one data set increases, while the other decreases), while the opposite is true if the vectors are pointing in the same direction. The score plot correlates the relationship between the aging scenarios and the direction of increasing exposure is indicated in the plots (→). Groupings of data points in each aging scenario in the score plots are indicative of insensitivity of the data to absorbed dose. The colored ellipses in the score plots are specific aging scenario regions with 95% confidence.

The variable correlation plot of Figure 28 will first be discussed. For XLPE, the characterization methods (or variables) demonstrate a strong correlation to the PCs. The grouping and positive correlation of CI and τ in the correlation plot indicate that these two characterization methods produce similar trends in the characterization data for XLPE; the orientation of these two methods along the PC1 direction may indicate that this axis is representative of oxidation. On the other hand, an inverse correlation was found between EAB and total color difference indicating that total color difference may be a valid metric, and non-destructive technique, to evaluate the lifetime of cable insulation in the field. Furthermore, measurement of the total color difference is a particularly advantageous technique because a trained individual can distinguish variations in total color difference in the range of 0.1 to 0.2 [51]; however, the prevalence of darker color cable insulation limits the applicability of this technique. Within expectations, IM is positioned nearly 90° to EAB indicating no correlation between the characterization methods – this result is not surprising as IM was found to be relatively insensitive to exposure for XLPE (see Figure 25). The orientation of Δm along PC2 may indicate that this direction primarily represents Δm during exposure. For EPDM, CI is again positioned on the PC1 axis with a positive loading, in agreement with the hypothesis that this axis may represent oxidation. Also similar to XLPE, EAB and total color difference were inversely correlated, further supporting the usage of total color difference as a metric to estimate cable insulation degradation in the field. A nearly inverse correlation is now observed for EAB and IM for EPDM, demonstrating that IM is a useful technique to detect cable insulation degradation in this material type. Unlike in XLPE, Δm and IM are inversely correlated for EPDM; therefore, it may be possible to extend to the results for the first aging step (T in $T+R$ and R in $R+T$) for Δm to determine the variations in IM for those same conditions.

The score plot of Figure 29 will now be discussed. For XLPE, the impact of a specific absorbed dose on specimens exposed to different aging scenarios is not homogeneous and is more substantial at lower doses (e.g., 20 kGy). Furthermore, both sequential aging scenarios ($T+R$ and $R+T$) vary significantly from the unaged specimen (+) at lower doses, while the simultaneous aging scenario (T/R) does not. The orientation of the T/R aging scenario along PC1 (data points are moving towards the right side of the plot with increasing exposure) may imply that more oxidation reactions are occurring with increasing exposure (in agreement with Figure 22). This also supports the hypothesis that degradation of XLPE for the $T+R$ aging scenario is not primarily due to oxidative reactions as this aging scenario was observed to produce the shortest lifetime. The orientation of the $T+R$ data along PC2 may indicate that the degradation mechanism along this PC is responsible for the reduced lifetime of XLPE, although the exact mechanism is difficult to interpret from Figure 28. For EPDM, PC1 is mostly correlated with increased exposure.

Opposite to that observed for XLPE, no significant variations are observed between the aging scenarios at low exposures. Interestingly, at high exposure (280 kGy or higher) the *R+T* aging scenario produces data that trends along the PC2 direction, which correlates with mechanical property changes (as seen by the orientation IM and τ in Figure 28). This result agrees with mechanical tests, such as IM and EAB, which were found to produce the most severe variations for the *R+T* aging scenario for EPDM.

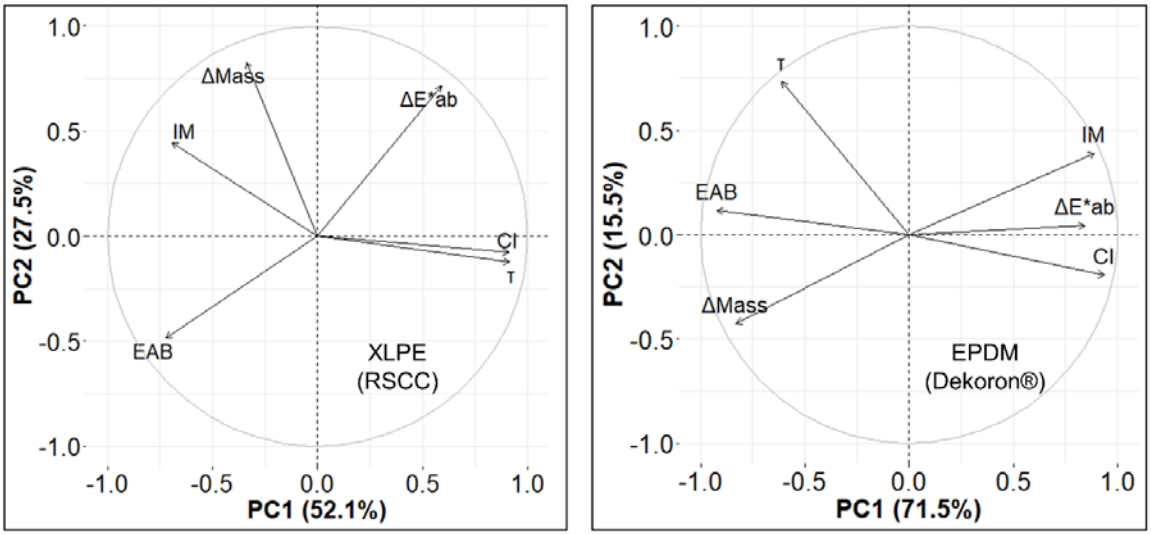

Figure 28. Variable correlation plot of PCA for the methods of Section 6 for (left) XLPE and (right) EPDM.

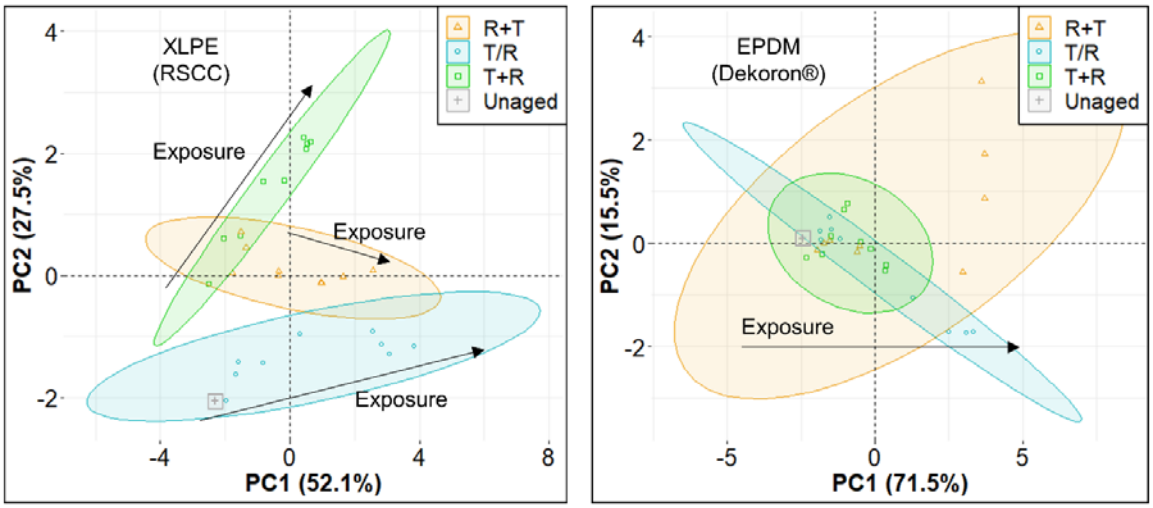

Figure 29. Score plot for PCA of the aging scenarios for (left) XLPE and (right) EPDM. The direction of increasing exposure is indicated on the plots and the unaged specimens are shown as +.

7.3 Sensitive Measures of Aging

In addition to metrics that correlate well to existing standards for cable degradation (such as total color difference as discussed in Section 7.2), preferred characterization techniques are also sensitive to cable degradation throughout the life of the material [47]. In this report, the sensitivity of the characterization technique is defined as the ratio of the aged specimen property to the unaged specimen property; thus, as cable specimens age, sensitive characterization techniques produce larger normalized variations in

measured properties. The normalized variations of the test metrics employed in this report are shown Figure 30. Here, as opposed to EAB, it was observed that the CI was the most sensitive test metric for most aging scenarios, followed by the total color difference. As a stronger correlation to EAB was observed for both XLPE and EPDM for total color difference, this characterization technique is possibly the most appropriate characterization technique.

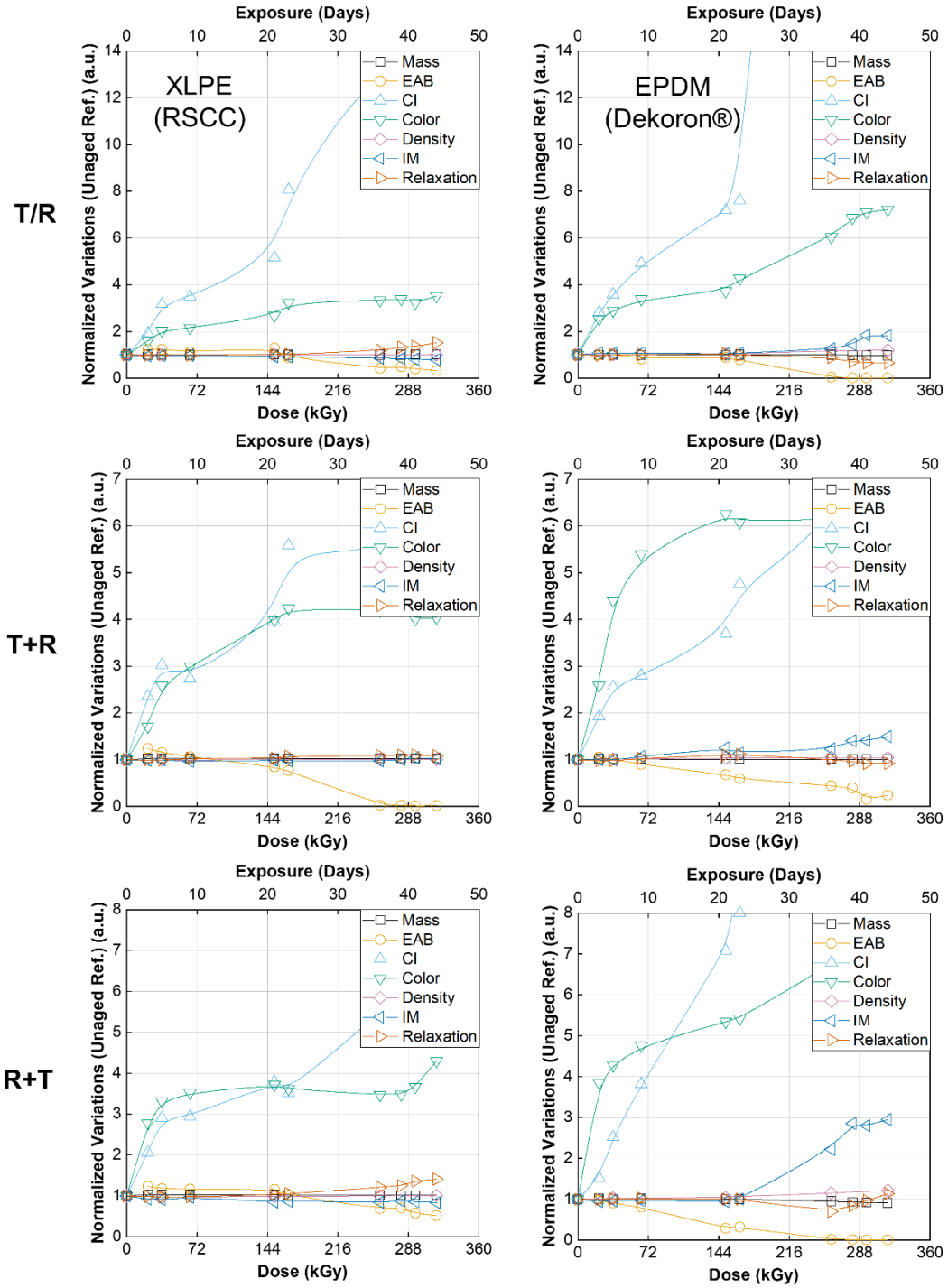

Figure 30. Normalized variations in the measured properties for aged insulation specimens: (left) XLPE and (right) EPDM.

7.4 Comparison to Previous Work

A summary of the lifetime predictions (EAB at 50% of the unaged specimen EAB, $e/e_0 = 0.5$) for the sequential aging scenarios with respect to the simultaneous aging scenario is shown in Table 12 for XLPE and EPDM. Prior exploration of the effects of sequential versus simultaneous aging on nuclear cable insulation was summarized in a report by Subudhi [3]. Direct comparison of previous work investigating the effect of aging scenarios to this work is difficult as previous efforts evaluated EAB for a single dose. Nevertheless, a summary of selected materials demonstrating previously measured normalized EAB (e/e_0) for different aging scenarios is shown in Table 13. As concluded by Subudhi [3], "for most materials, simultaneous simulation causes the severest degradation compared to any sequential methods." For the materials, dose rate, and temperature investigated in this work, the simultaneous aging scenario was not found to be the most severe case. As discussed in Section 6.2, lifetime differed based upon material type and aging scenario. A reduced insulation lifetime was found for XLPE for the *T*+*R* aging scenario when compared to the simultaneous aging scenario. On the other hand, in comparison to the simultaneous aging scenario, a reduced lifetime was found for the *R*+*T* aging scenario for EPDM.

Table 12. Lifetime prediction of sequential aging scenarios normalized to the simultaneous aging scenario.

Type	Aging Scenario	Ratio at $e/e_0 = 0.5$ to Simultaneous (*T*/*R*) (%)	Dose (kGy)	Temperature (°C)	Exposure (Days)
XLPE (RSCC)	*T*+*R*	74	203	150	28
	R+*T*	116	320	150	44
EPDM (Dekoron®)	*T*+*R*	111	225	150	31
	R+*T*	64	130	150	18

EPDM = ethylene-propylene-diene elastomer; XLPE = cross-linked polyethylene. At 300 Gy/hr and *T*/*R* at a dose of 276 kGy for XLPE and 203 kGy for EPDM ($e/e_0 = 0.5$).

Table 13. Previous work, with sequential aging normalized to the simultaneous aging scenario (*T*/*R*) [3].

Material	Aging Scenario	e/e_0	Ratio to Simultaneous (*T*/*R*) (%)	Dose Rate (Gy/hr)	Dose (kGy)	Temperature (°C)	Exposure (Days)
EPR-1483 [52]	*T*/*R*	0.41	-	600	430	120	30
	T+*R*	0.47	115	650	440	120	28
	R+*T*	0.41	100	650	440	120	28
EPR-B [52]	*T*/*R*	0.30	-	2600	440	139	7
	T+*R*	0.45	150	2600	440	139	7
	R+*T*	0.52	173	2600	440	139	7
CSPE [53]	*T*/*R*	0.15	-	650	250	120	16
	T+*R*	0.45	300	650	250	120	16
	R+*T*	0.25	167	650	250	120	16
XLPO-1 [53]	*T*/*R*	0.60	-	650	250	120	16
	T+*R*	0.75	125	650	250	120	16
	R+*T*	0.75	125	650	250	120	16

EPR = ethylene-propylene rubber; CSPE = chlorosulfonated polyethylene; CPE = chlorinated polyethylene elastomer; XLPO = cross-linked polyolefin.

8. CONCLUSIONS

The objective of this report is to address one of the four cable aging knowledge gaps, synergistic effects, emphasized by Fifield et al. [8]. Here, synergistic effects refer to polymer aging mechanisms due to simultaneous or concurrent application of thermal and gamma radiation stresses, which may differ from sequentially applied thermal and radiation stresses. Previously, it was suggested that cable degradation may be more severe with simultaneous aging than with sequential aging [3,5]. This has led to concern that the historical practice of applying sequential aging (thermal followed by irradiation) [3] to estimate cable lifetime may not accurately reflect the simultaneous exposure of in-service conditions.

In this report, two of the most common low-voltage electrical cable insulation material types in nuclear containment, XLPE and EPDM, were selected to investigate the effects of stress exposure sequence. Accelerated aging experiments were conducted at consistent dose rate and temperature to better understand cable degradation based solely on the order of stress sequence. The gamma dose rate, total dose, and temperature were selected based upon input from stakeholders and resource constraints. Characterization methods including mass change, elongation at break, carbonyl index, total color difference, density, indenter modulus, and relaxation constant were selected to quantify the severity of the selected aging scenarios: (1) simultaneous [*T/R*, thermal and irradiation], (2) sequential [*T*+*R*, thermal followed by irradiation], and (3) sequential [*R*+*T*, irradiation followed by thermal]. In addition, to better understand the degradation mechanisms of the selected aging scenarios, a nonlinear reaction kinetics approach developed by Gillen et al. [40] and principal component analysis were employed.

The characterization results yield insights into lifetime prediction and degradation mechanisms of low-voltage nuclear instrumentation cables. Most significantly, sequential aging was found to produce a different operational lifetime (defined as time to 50% of the unaged specimen EAB) when compared to simultaneous aging that varied with the material type and aging scenario as shown in Table 12:

- For XLPE, lifetimes were found to be less than the simultaneous aging scenario for the sequential thermal followed by irradiation aging, but greater for the sequential irradiation followed by thermal aging ($T+R < T/R < R+T$). The degradation mechanism for the *T*+*R* aging scenario was found to be complicated as oxidation does not appear to dominate the degradation. In addition to a reduced carbonyl index, principal component analysis of the *T*+*R* aging scenario revealed a strong correlation to the second principal component, as opposed to the first principal component which is hypothesized to represent oxidation. This may indicate that further cross-linking, as opposed to oxidation, is responsible for the degradation of the most severe aging scenario for XLPE.
- For EPDM, lifetimes were found to be less than the simultaneous aging scenario for the sequential irradiation followed by thermal aging, but greater for the sequential thermal followed by irradiation aging ($R+T < T/R < T+R$). The rate of hydroperoxide breakdown was modeled for elongation at break, carbonyl index, indenter modulus, and density to be least for the *T*+*R* aging scenario, followed by the *R*+*T* aging scenario, and then the *T/R* aging scenario. Due to an extended induction period observed for the *T/R* aging scenario, potentially due to competition between side reactions and the overall termination reaction, the most severe aging scenario for EPDM was found to be *R*+*T*.

The results of this work suggest that the sequential aging commonly used in cable qualification may be conservative relative to in-service aging and that conclusions regarding that conservatism likely require addition consideration of the specific materials and conditions in question. This report also demonstrates that mass change may be a useful technique for estimating the degradation of cables insulated with EPDM, particularly with the simultaneous (*T/R*) and sequential irradiation followed by thermal (*R*+*T*) aging scenarios, because a sharp decrease in mass was observed to correlate to a reduction in EAB. In addition, total color difference was observed to be possibly advantageous for non-destructive characterization based on principal component analysis correlation between elongation at break and total color difference, and based on the sensitivity of the technique.

9. REFERENCES

[1] NRC, Expanded Materials Degradation Assessment (EMDA), Volume 1 : Executive Summary of EMDA Process and Results, NUREG/CR-7153, 2013. https://www.nrc.gov/docs/ML1427/ML14279A321.pdf

[2] P.L. Joskow, The Future of nuclear power in the United States: Economic and regulatory challenges, MIT-CEEPR 06-019WP, (2006). https://dspace.mit.edu/bitstream/handle/1721.1/45065/2006-019.pdf?sequence=1&isAllowed=y

[3] M. Subudhi, Literature Review of Environmental Qualification of Safety-Related Electric Cables. Vol.1 Summary of Past Work, (1996) NUREG/CR-6384, BNL-NUREG-52480, 1–306. https://www.nrc.gov/reading-rm/doc-collections/nuregs/contract/cr6384/v1/part1/

[4] R.F. Gazdzinski, W.M. Denny, G.J. Toman, R.T. Butwin, SAND96-0344: Aging Managment Guideline for Commercial Nuclear Power Plants - Electrical Cble and Terminations, 2000. https://www.nrc.gov/docs/ML0311/ML031140264.pdf

[5] NRC, Expanded Materials Degradation Assessment (EMDA), Volume 5: Aging of Cables and Cable Systems, NUREG/CR-7153, 2014. https://www.nrc.gov/docs/ML1427/ML14279A461.pdf

[6] Nuclear Energy Agency - Committee on the Safety of Nuclear Installations, NEA/CSNI/R(2018)8 Cable Ageing in Nuclear Power Plants, 2018. https://www.oecd-nea.org/upload/docs/application/pdf/2020-01/dir1/csni-r2018-8.pdf

[7] K.L. Simmons, P. Ramuhalli, D.L. Brenchley, J.B. Coble, H. Hashemian, R. Konnik, S. Ray. Light Water Reactor Sustainability (LWRS) Program – Non-Destructive Evaluation (NDE) R&D Roadmap for Determining Remaining Useful Life of Aging Cables in Nuclear Power Plants. United States: N. p., 2012. Web. doi:10.2172/1097978. https://doi.org/10.2172/1097978

[8] L.S. Fifield, A. Zwoster, M. Murphy, PNNL-27987: Initiation of Experimental Campaign to Address Knowledge Gaps Related to Simultaneous Thermal and Gamma Radiation Aging of Crosslinked Polyethylene and Ethylene-Propylene Rubber Cable Insulation, Richland, WA, 2018.

[9] K.T. Gillen, R.L. Clough, Rigorous experimental confirmation of a theoretical model for diffusion-limited oxidation, *Polymer* (Guildf). 33 (1992) 4358–4365. https://doi.org/10.1016/0032-3861(92)90280-A.

[10] L. Verardi, D. Fabiani, G.C. Montanari, Correlation of electrical and mechanical properties in accelerated aging of LV nuclear power plant cables, *ICHVE 2014 - 2014 Int. Conf. High Volt. Eng. Appl.* (2014) 1–4. https://doi.org/10.1109/ICHVE.2014.7035376.

[11] K.T. Gillen, R.L. Clough, Time-temperature-dose rate superposition: A methodology for extrapolating accelerated radiation aging data to low dose rate conditions, *Polym. Degrad. Stab.* 24 (1989) 137–168. https://doi.org/10.1016/0141-3910(89)90108-0.

[12] G. Przybytniak, J. Boguski, V. Placek, L. Verardi, D. Fabiani, E. Linde, U.W. Gedde, Inverse effect in simultaneous thermal and radiation aging of EVA insulation, *Express Polym. Lett.* 9 (2015) 384–393. https://doi.org/10.3144/expresspolymlett.2015.36.

[13] K.T. Gillen, Importance of Synergism for Degradation of Elastomers in Combined Radiation Plus Temperature Environments, *Rubber Chem. Technol*. 93 (2019) 121–141. https://doi.org/10.5254/rct.19.80457.

[14] T. Seguchi, K. Tamura, T. Ohshima, A. Shimada, H. Kudoh, Degradation mechanisms of cable insulation materials during radiation-thermal ageing in radiation environment, *Radiat. Phys. Chem.* 80 (2011) 268–273. https://doi.org/10.1016/j.radphyschem.2010.07.045.

[15] T. Seguchi, K. Tamura, H. Kudoh, A. Shimada, M. Sugimoto, Degradation of cable insulation material by accelerated thermal radiation combined ageing, *IEEE Trans. Dielectr. Electr. Insul*. 22 (2015) 3197–3206. https://doi.org/10.1109/TDEI.2015.004880.

[16] M. Ito, Service Life Prediction of Polymeric Materials, Springer US, Boston, MA, 2009. https://doi.org/10.1007/978-0-387-84876-1.

[17] M.T. Shaw, Y.M. Liu, Modeling of thermal and radiative aging of polymeric cable materials, Conf. Rec. *IEEE Int. Symp. Electr. Insul.* 2 (1996) 638–641.

https://doi.org/10.1109/elinsl.1996.549426.
[18] DOE, Aging management guideline for commercial nuclear power plants - electrical cable and terminations, SAND96-0344. (1996). http://www.osti.gov/energycitations/product.biblio.jsp?osti_id=204243.
[19] ASTM, D1418 Standard Practice for Rubber and Rubber Latices - Nomenclature, West Conshohocken, PA, 2017. https://doi.org/10.1520/D1418-17.
[20] M.F. Sheridan, ed., The Vanderbilt Rubber Handbook, 14th Edition, R. T. Vanderbilt, Norwalk, CT, 2010.
[21] P. Hu, P.P. Zhao, G.W. Zhang, X.H. Wang, Thermal properties of 60Co irradiated crosslinked high density polyethylene, *Sol. Energy Mater. Sol. Cells.* 149 (2016) 55–59. https://doi.org/10.1016/j.solmat.2015.12.042.
[22] A.R. Amin, Synergistic effect of TNPP and carbon black in weathered XLPE materials, *J. Polym. Environ.* 17 (2009) 267–272. https://doi.org/10.1007/s10924-009-0148-5.
[23] R. Kochetov, T. Christen, F. Gullo, FTIR analysis of LDPE and XLPE thin samples pressed between different protective anti-Adhesive films, *ICEMPE 2017 - 1st Int. Conf. Electr. Mater. Power Equip*. (2017) 49–52. https://doi.org/10.1109/ICEMPE.2017.7982097.
[24] Q. Zhao, X. Li, J. Gao, Aging of ethylene-propylene-diene monomer (EPDM) in artificial weathering environment, *Polym. Degrad. Stab*. 92 (2007) 1841–1846. https://doi.org/10.1016/j.polymdegradstab.2007.07.001.
[25] M. Tefferi, Z. Li, Y. Cao, H. Uehara, Q. Chen, Novel EPR-insulated DC cables for future multi-terminal MVDC integration, *IEEE Electr. Insul. Mag*. 35 (2019) 20–27. https://doi.org/10.1109/MEI.2019.8804331.
[26] F.J. Linnig, J.E. Stewart, Infrared study of some structural changes in natural rubber during vulcanization, *J. Res. Natl. Bur. Stand*. (1934). 60 (1958) 9. https://doi.org/10.6028/jres.060.002.
[27] L. Guadagno, P. Longo, M. Raimondo, C. Naddeo, A. Mariconda, V. Vittoria, G. Iannuzzo, S. Russo, Use of Hoveyda-Grubbs' second generation catalyst in self-healing epoxy mixtures, *Compos. Part B Eng.* 42 (2011) 296–301. https://doi.org/10.1016/j.compositesb.2010.10.011.
[28] S. Mitra, A. Ghanbari-Siahkali, P. Kingshott, S. Hvilsted, K. Almdal, An investigation on changes in chemical properties of pure ethylene-propylene-diene rubber in aqueous acidic environments, *Mater. Chem. Phys*. 98 (2006) 248–255. https://doi.org/10.1016/j.matchemphys.2005.09.028.
[29] L. Greenspan, Humidity fixed points of binary saturated aqueous solutions, *J. Res. Natl. Bur. Stand. Sect. A Phys. Chem*. 81A (1977) 89. https://doi.org/10.6028/jres.081A.011.
[30] IEC/IEEE 62582-3: 2012, Nuclear power plants - Instrumentation and control important to safety - Electrical equipment condition monitoring methods - Part 3: Elongation at break, International Electrotechnical Commission, Geneva, Switzerland, 2012. https://doi.org/10.3403/30189461.
[31] S.G. Kazarian, K.L.A. Chan, ATR-FTIR spectroscopic imaging: Recent advances and applications to biological systems, *Analyst*. 138 (2013) 1940–1951. https://doi.org/10.1039/c3an36865c.
[32] D. Fassini, A.R.C. Duarte, R.L. Reis, T.H. Silva, Bioinspiring chondrosia reniformis (Nardo, 1847) collagen-based hydrogel: A new extraction method to obtain a sticky and self-healing collagenous material, *Mar. Drugs*. 15 (2017). https://doi.org/10.3390/md15120380.
[33] P.S. Thomas, J.P. Guerbois, G.F. Russell, B.J. Briscoe, FTIR study of the thermal degradation of poly(vinyl alcohol), *J. Therm. Anal. Calorim*. 64 (2001) 501–508. https://doi.org/10.1023/A:1011578514047.
[34] J. Troscianko, Empirical Imaging, (2020). http://www.empiricalimaging.com/ (accessed January 23, 2020).
[35] J. Troscianko, M. Stevens, Image calibration and analysis toolbox - a free software suite for objectively measuring reflectance, colour and pattern, *Methods Ecol. Evol*. 6 (2015) 1320–1331. https://doi.org/10.1111/2041-210X.12439.
[36] S.A. Burns, Generating Reflectance Curves from sRGB Triplets, (2017) 1–39. http://scottburns.us/reflectance-curves-from-srgb/.
[37] ASTM D792-13, Standard Test Methods for Density and Specific Gravity (Relative Density) of

Plastics by Displacement, West Conshohocken, PA, 2013. https://doi.org/10.1520/D0792-13.2.
[38] S. Liu, Fifield L.S., Bowler N. (2019) Aging Mechanisms and Nondestructive Aging Indicator of Filled Cross-Linked Polyethylene (XLPE) Exposed to Simultaneous Thermal and Gamma Radiation. In: Jackson J., Paraventi D., Wright M. (eds) *Proceedings of the 18th International Conference on Environmental Degradation of Materials in Nuclear Power Systems – Water Reactors.* The Minerals, Metals & Materials Series. Springer, Cham. https://doi.org/10.1007/978-3-030-04639-2_82
[39] B. Moon, N. Jun, S. Park, C.S. Seok, U.S. Hong, A study on the modified Arrhenius equation using the oxygen permeation block model of crosslink structure, *Polymers* (Basel). 11 (2019). https://doi.org/10.3390/polym11010136.
[40] K.T. Gillen, R.L. Clough, A kinetic model for predicting oxidative degradation rates in combined radiation-thermal environments, *J. Polym. Sci. Polym. Chem. Ed*. 23 (1985) 2683–2707. https://doi.org/10.1002/pol.1985.170231011.
[41] R.L. Clough, K.T. Gillen, Combined Environment Aging Effects: Radiation-Thermal Degradation of Polyvinylchloride and Polyethylene., *J. Polym. Sci.* A1. 19 (1981) 2041–2051. https://doi.org/10.1002/pol.1981.170190816.
[42] G. James, D. Witten, T. Hastie, R. Tibshirani, An Introduction to Statistical Learning, Springer New York, New York, NY, 2013. https://doi.org/10.1007/978-1-4614-7138-7.
[43] S. Lê, J. Josse, F. Husson, FactoMineR : An R Package for Multivariate Analysis, *J. Stat. Softw.* 25 (2008). https://doi.org/10.18637/jss.v025.i01.
[44] C.C. De Silva, Beckman S.P., Liu S., Bowler N. (2019) Principal Component Analysis (PCA) as a Statistical Tool for Identifying Key Indicators of Nuclear Power Plant Cable Insulation Degradation. In: Jackson J., Paraventi D., Wright M. (eds) *Proceedings of the 18th International Conference on Environmental Degradation of Materials in Nuclear Power Systems – Water Reactors.* The Minerals, Metals & Materials Series. Springer, Cham. https://doi.org/10.1007/978-3-030-04639-2_78
[45] M. Rahaman, A. Aldalbahi, P. Govindasami, N.P. Khanam, S. Bhandari, P. Feng, T. Altalhi, A new insight in determining the percolation threshold of electrical conductivity for extrinsically conducting polymer composites through different sigmoidal models, *Polymers* (Basel). 9 (2017) 1–17. https://doi.org/10.3390/polym9100527.
[46] R. Steffen, H. Setyamukti, G. Wallner, K. Geretschläger, B. Röder, Kinetics of degradation-induced polymer luminescence: Polyamide under dry heat exposure, *Polym. Degrad. Stab*. 140 (2017) 114–125. https://doi.org/10.1016/j.polymdegradstab.2017.04.010.
[47] F.M. Guérout, R.G. Boor, Development of indentation techniques in support of cable condition monitoring programs, *IEEE Trans. Dielectr. Electr. Insul*. 22 (2015) 2818–2825. https://doi.org/10.1109/TDEI.2015.004612.
[48] S. Liu, S.W. Veysey, L.S. Fifield, N. Bowler, Quantitative analysis of changes in antioxidant in crosslinked polyethylene (XLPE) cable insulation material exposed to heat and gamma radiation, P*olym. Degrad. Stab.* 156 (2018) 252–258. https://doi.org/10.1016/j.polymdegradstab.2018.09.011.
[49] G. Teissedre, J.F. Pilichowski, S. Chmela, J. Lacoste, Ageing of EPDM - I: Photo and thermal stability of EPDM hydroperoxides, *Polym. Degrad. Stab*. 53 (1996) 207–215. https://doi.org/10.1016/0141-3910(96)00082-1.
[50] Y.S. Cho, M.J. Shim, S.W. Kim, Thermal degradation kinetics of PE by the Kissinger equation, Mater. Chem. Phys. 52 (1998) 94–97. https://doi.org/10.1016/S0254-0584(98)80013-8.
[51] G. Iannuzzi, B. Mattsson, M. Rigdahl, Color changes due to thermal ageing and artificial weathering of pigmented and textured ABS, *Polym. Eng. Sci.* 53 (2013) 1687–1695. https://doi.org/10.1002/pen.23438.
[52] L.D. Bustard, Ethylene Propylene Cable Degradation During LOCA Research Tests: Tensile Properties at the Completion of Accelerated Aging, NUREG/CR-3538, SAND83-1258, Off. Nucl. Regul. Res. U.S. Nucl. Regul. Comm. (1982).

https://www.nrc.gov/docs/ML1335/ML13357A667.pdf
[53] L.D. Bustard, The effect of thermal and irradiation aging simulation procedures on polymer properties, NUREG/CR-3629, SAND83-2651, Off. Nucl. Regul. Res. U.S. Nucl. Regul. Comm. (1984). https://www.nrc.gov/docs/ML0622/ML062260295.pdf